Gravity anomalies and crustal structure at the southeast Greenland margin

Jun Korenaga

Department of Earth, Atmospheric, and Planetary Sciences, Massachusetts Institute of Technology, Cambridge

W. Steven Holbrook

Department of Geology and Geophysics, University of Wyoming, Laramie, Wyoming

Robert S. Detrick and Peter B. Kelemen

Department of Geology and Geophysics, Woods Hole Oceanographic Institution
Woods Hole, Massachusetts

Abstract. Free-air gravity anomalies across the southeast Greenland margin are investigated in conjunction with a well-constrained seismic velocity model to provide a constraint on subsurface density structure. This volcanic rifted margin is characterized by the presence of ~30-km-thick igneous crust, which correlates with a positive gravity high of ~60 mGal. A new systematic approach is adopted for gravity modeling, which consists of (1) full error propagation from the velocity model to predicted gravity anomalies through a posteriori model covariance represented by Monte Carlo ensembles, (2) the inversion of residual gravity anomalies for density variations within geological subdomains, and (3) the joint inversion of seismic travel times and gravity anomalies. A density model derived from the velocity model, using conventional conversion laws for the continental and oceanic crust, substantially underpredicts the observed gravity by ~70 mGal over the continental shelf. Neither errors in the velocity model nor the uncertainty of the chosen conversion laws are shown to be sufficient for such a large gravity misfit. A possible range of mantle contribution is first investigated by modeling various thermal evolution and depletion scenarios, which suggests that the maximum contribution is only ~20 mGal, assuming constant source mantle composition throughout continental rifting and subsequent seafloor spreading. If most of the residual gravity anomaly has a crustal origin, applying a conversion law with a denser upper crust in the continent-ocean transition zone seems to be the only plausible option to resolve this difficulty. Contrasting eruption environments for the transition zone crust (subaerial) and the oceanic crust (submarine) probably result in different porosity structures, to which a velocity-density relationship is highly sensitive. The wire log and laboratory measurements of plateau basalts recovered from recent drilling legs on North Atlantic margins seem to support this explanation. An alternative explanation, which invokes a strong degree of source mantle heterogeneity, is also plausible on the basis of a recent geochemical study of the North Atlantic igneous province.

1. Introduction

In the past decade or so, there have been an increasing number of deep crustal seismic investigations on rifted continental margins, which have often revealed thick igneous crust at continent-ocean transition zones [*LASE Study Group*, 1986; *White et al.*, 1987; *Mutter and Zehnder*, 1988; *Tréhu et al.*, 1989; *Zehnder et al.*, 1990; *Hopper et al.*, 1992; *Holbrook and Kelemen*, 1993; *Schlindwein and Jokat*, 2000]. The thick igneous crust at these volcanic passive margins is typically 20-30 km thick, and its lower-crustal velocity is usually higher than 7.2 km s^{-1}. The correlation between the velocity and density of crustal rocks [*Birch*, 1961] implies the existence of a corresponding high-density lower crust, which has been used to

explain positive gravity anomalies observed at the continent-ocean transition zones [*Morgan and Barton*, 1990; *Holbrook et al.*, 1994a,b; *Lizarralde and Holbrook*, 1997]. The high-velocity and high-density crust indicates an unusually high MgO content compared to the normal oceanic crust, implying the melting of hotter mantle during continental breakup [e.g., *White and McKenzie*, 1989; *Kelemen and Holbrook*, 1995].

In 1996, deep seismic experiments were conducted across the southeast Greenland margin to systematically investigate the margin crustal structure with respect to the presumed Iceland hot spot track (W. S. Holbrook et al., Mantle thermal structure and melting processes during continental breakup in the North Atlantic, submitted to *Earth and Planetary Science Letters*, 2000, hereinafter cited as W. S. Holbrook et al., submitted manuscript, 2000), and one of the seismic transects (transect 2) has been analyzed with joint refraction and reflection tomography to construct a high-fidelity seismic velocity model [*Korenaga et al.*, 2000]. Transect 2 was located ~250 km south of the Iceland hot spot track (Figure 1a) and extended from the deep-water ocean
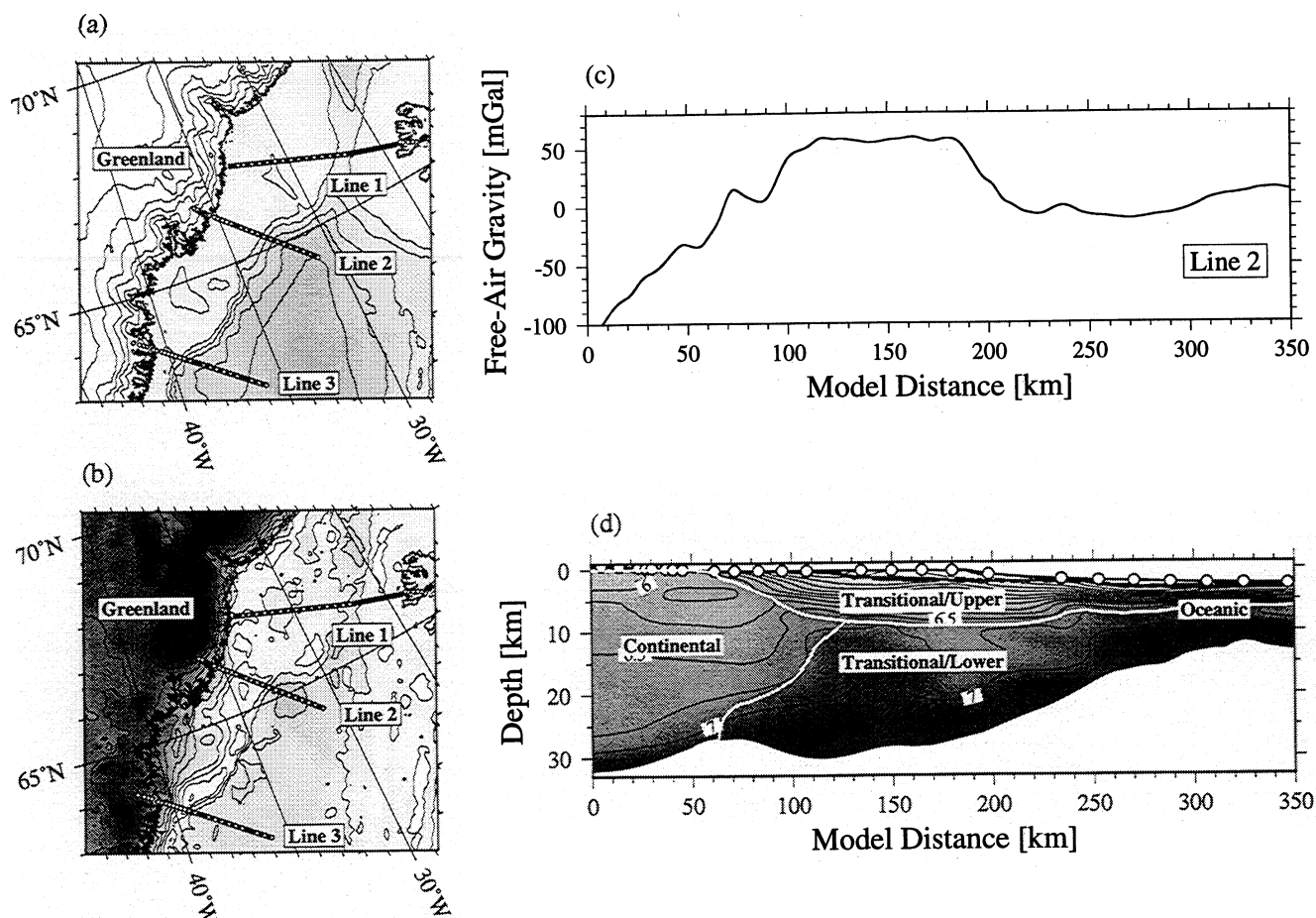
Figure 1. (a) Bathymetry map with location of 1996 SIGMA seismic transects. Contour interval is 500 m. Solid lines denote air gun shot lines, whereas open circles denote onshore/offshore seismic instruments. (b) Free-air gravity anomaly map with contour interval of 25 mGal. (c) Free-air gravity anomaly on transect 2. Land data (<km 50) were applied with Bouguer correction. (d) P wave crustal velocity model for transect 2, with geological interpretation of continent-ocean transition zone [*Korenaga et al.*, 2000].

basin, across the continental slope and shelf, to the coastal region. The free-air gravity anomaly along the transect is marked by a positive gravity high with an amplitude of ~60 mGal over the continental shelf (Figure 1b), which is also characteristic of gravity anomalies at other North Atlantic margins [e.g., *Morgan and Barton*, 1990]. There is significant lateral variation in crustal thickness along the transect, from ~9 km at the seaward end to ~30 km beneath the continental shelf (Figure 1c). Whereas a water-crust density contrast at the shallowing bathymetry produces a positive gravity anomaly, a crust-mantle density contrast at this deepening Moho results in a larger anomaly with an opposite sign. The observed gravity high thus requires a variation in crustal density that can offset the effect of crustal thickening. The P wave velocity of the thick igneous lower crust is, however, only ~7.0 km s^{-1} on average and not significantly higher than the thinner oceanic crust, so that there is an apparent discrepancy between the velocity model and the observed free-air gravity anomaly on transect 2.

The crustal velocity structure of transect 2 is well constrained by the unprecedented quality of seismic data with a dense receiver array and deep-penetrating sources, and its reliability has been comprehensively demonstrated by a nonlinear Monte Carlo uncertainty analysis [*Korenaga et al.*, 2000]. Therefore we have an opportunity to resolve the possible origin of the conspicuous gravity high, which may also be applicable to other volcanic

margins. The purpose of this paper is to construct a density model that is consistent with both the observed free-air gravity anomaly and the crustal velocity structure and to discuss the geological and geophysical implications of the inferred density structure. Though inference on density structure solely from gravity anomalies is notoriously nonunique, it is possible to considerably reduce the nonuniqueness and to place reasonable bounds on our estimate of density structure by utilizing the seismic velocity information and by considering possible geological processes involved in the formation of a volcanic passive margin. Our approach is based on (1) the full characterization of the absolute uncertainty of the velocity model [*Korenaga et al.*, 2000], which enables us to isolate other sources of uncertainty in regional gravity modeling, and (2) the inversion of residual gravity anomalies for density variation within a variable-shaped domain. We begin with a critical evaluation of existing velocity-density relationships for igneous rocks, which is fundamental to the use of a seismic velocity model as a constraint on density structure.

2. Paradox of the Margin Gravity High

The gravity profile along transect 2 was constructed by combining shipboard free-air gravity data and Bouguer-corrected land gravity data; high-resolution marine gravity data based on satellite altimetry are also available [*Smith and Sandwell*, 1995],

which are virtually identical with the shipboard data except at very short wavelengths (<1-2 km). Because the land data included a Bouguer correction, we will consider only a subhorizontal region to model the observed gravity anomaly. Density models are 350 km wide and 35 km deep and are gridded with uniform rectangular cells, each of which is 200 m wide and 50 m deep, to accurately represent sharp density discontinuities such as the seafloor and the Moho. We assume that observed gravity anomalies can be modeled in two dimensions with reasonable accuracy, since gravity anomalies and bathymetry both have nearly linear patterns aligned perpendicular to transect 2 (Figures 1a and 1b). Though there are three-dimensional variations both in bathymetry and basement topography associated with bulging of continental shelf at >50 km to northwest [Tucholke, 1986], their influence on transect 2 is negligible because a gravity anomaly has a horizontal decay length comparable to its source depth. With no information on the across-transect variation of crustal structure, however, the assumed two dimensionality of deep crustal structure is left for future validation. Gravity anomalies are obtained as the vertical integral of contributions from horizontal density layers, each of which is calculated in the one-dimensional (1-D) Fourier domain [e.g., Blakely, 1995]. The horizontal ends of the model are continuously padded for an additional 200 km to avoid truncation artifacts, and the model was then mirrored to minimize the leaking of a linear trend into shorter wavelengths within the Fourier transform. We bench marked our gravity calculations against various analytical solutions for simple bodies [e.g., Telford et al., 1990], and the numerical errors were found to be <1%. In all gravity calculations in this paper, a reference density structure is taken from km ~300 to match the predicted anomaly with the observed anomaly toward the seaward end of the transect.

We first considered a density model comprised of four constant density layers: water (1.0 Mg m^{-3}), sediment (2.0 Mg m^{-3}), crust (2.86 Mg m^{-3}), and mantle (3.3 Mg m^{-3}). The basement and Moho boundaries are adopted from the seismic velocity model. A gravity anomaly calculated from this simple density model largely underpredicts the observed gravity anomaly, especially for the positive gravity high observed over the continental shelf (Figure 2). This clearly illustrates that the effect of the deepening Moho along the transect is significantly larger than the effect of the shallowing bathymetry, despite the fact that the seafloor has a larger density contrast and is located closer to the surface. Thus strong density variations somewhere in the crust or mantle are necessary to explain the observed gravity anomaly. We will consider crustal density variations first, based on the seismic velocity model, and to do so, a conversion rule from P wave velocity to density needs to be determined. For the sedimentary layer we use Hamilton's [1978] empirical relation for shale, $\rho = 0.917 + 0.747V_p - 0.08V_p^2$, which is the best fit to data on the Ocean Drilling Program (ODP) Leg 152 sediment core [Larsen et al., 1994]. For the continental crust we use a nonlinear velocity-density regression curve estimated for average continental crust at 20 km depth [Christensen and Mooney, 1995], $\rho = 5.055 - 14.094/V_p$, throughout the whole continental crust; this crude application of the conversion law is not very critical because of the relatively uniform crustal thickness and the weak velocity heterogeneity within the continental crust. The high velocity gradients observed in the upper crust in the transition zone and oceanic regions are most likely due to the effects of porosity and alteration, and we use the following empirical relation, $\rho = 3.61 - 6.0/V_p$, which is based on Deep Sea Drilling Project (DSDP) and ODP core data [Carlson and Herrick, 1990].

The lower crust in the transition zone and oceanic regions occupies the largest volume in the model, so a conversion law for this subdomain probably has the most significant influence on the predicted gravity anomaly. The velocity-density systematics for igneous lower crust, however, have not been firmly established.
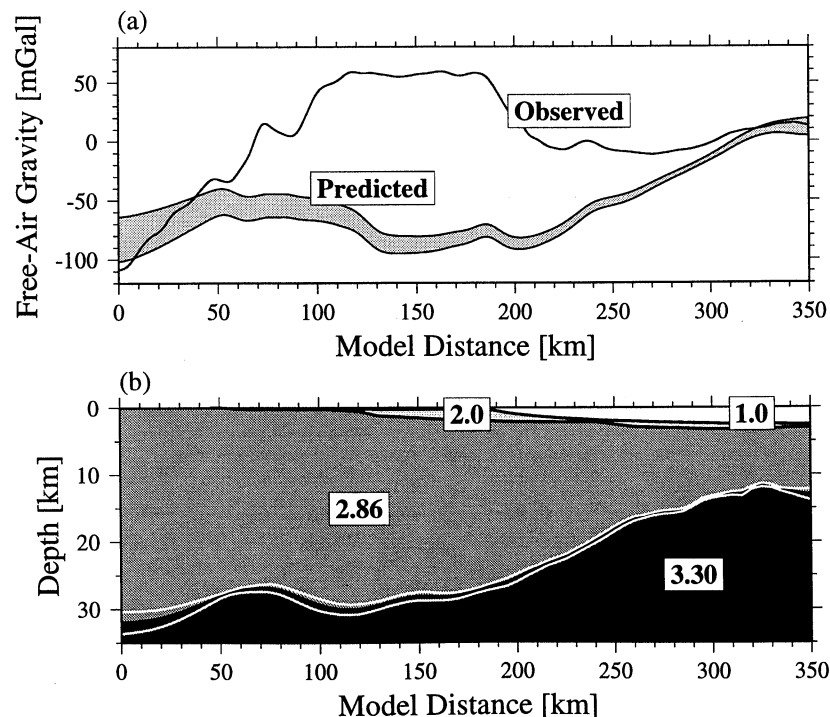

Figure 2. (a) Observed free-air gravity anomaly is plotted with predicted free-air gravity anomaly (±1σ) based on (b) four-layer constant density model. Standard deviation of predicted gravity anomaly is based on standard deviation of the Moho depths, as shown as white lines.

This is because laboratory measurements of velocity and density are mostly limited to gabbroic rocks sampled from the oceanic crust and ophiolites [e.g., *Christensen and Shaw*, 1970; *Christensen and Salisbury*, 1975; *Christensen and Smewing*, 1981], whose velocity is usually strongly affected by metamorphism and porosity. Whereas empirical relations based on these data are probably appropriate for the normal oceanic crust, the majority of which seems to be influenced by hydrothermal circulation [e.g., *Christensen and Salisbury*, 1975; *Gregory and Taylor*, 1981; *McCollom and Shock*, 1998] (see also J. Korenaga et al, Methods for resolving the origin of large igneous provinces from crustal seismology, submitted to *Journal of Geophysical Research*, 2000, hereinafter cited as J. Korenaga et al., submitted manuscript, 2000), it is not certain whether they are also applicable to the lower section of thick (>15 km) igneous crust, where crack-free, pristine gabbroic rocks unaffected by hydrothermal circulation probably predominate. In addition, though rock types expected for igneous lower crust are much more limited than those for continental crust [*Christensen and Mooney*, 1995], even mineral assemblages composed only of olivine, plagioclase, and clinopyroxene can have considerable compositional diversity, for which a single velocity to density conversion may not be appropriate.

To investigate the relationship between velocity and density expected for primary gabbroic rocks, we have conducted fractional crystallization modeling starting from several primary mantle melt compositions, corresponding to a wide range of mean pressures and mean fractions of melting. Because the chemical composition of igneous lower crust must be bounded by the composition of primary mantle melts and that of fractionated, "cumulate" mineral assemblages, by conducting the crystallization modeling at a range of crustal pressures, we should be able to delineate the permissible extent of velocity and density variation for igneous lower crust. Readers are referred to J. Korenaga et al. (submitted manuscript, 2000) for the details of the modeling procedures. The results are presented in Figure 3, with other published empirical relations for mafic and ultramafic rocks. In this modeling, we assume that seismic anisotropy is insignificant for igneous lower crust, in which the degree of anisotropy is unknown. For a given density, fractionated assemblages usually have higher velocity than unfractionated ones because FeO is preferentially partitioned into residual liquids. The observed scatter in the velocity-density diagram results from nonlinearity in mixing the elastic properties of different minerals. Note that all crack-free, synthetic assemblages lack the most commonly observed velocity-density values for normal oceanic crust (6.9 km s^{-1} and 2.9 Mg m^{-3}). Birch's law for rocks with mean atomic weight of ~21 [*Birch*, 1961] is broadly consistent with the modeling results. Since we are interested in explaining the gravity variation as a result of crustal density variation, we adopt *Birch*'s [1961] law for diabase, gabbro, and eclogite, $\rho = 0.375 + 0.375 V_p$, which can serve as an upper bound for the density of primary gabbroic rocks (Figure 3). For velocities of 6.8-7.0 km s^{-1} this conversion law is very close to traditional empirical relationships for the oceanic crust [e.g., *Christensen and Shaw*, 1970; *Carlson and Herrick*, 1990], so this upper bound only becomes significant for higher velocities. For the lowermost section of thick igneous crust, there is a possibility of garnet growth [*Ringwood and Green*, 1964,1966]. For anhydrous igneous rocks with a typical cooling history, however, this garnet growth is unlikely because of kinetic barriers to reaction [*Ahrens and Schubert*, 1975]. Even if garnet forms, the velocity and density of resultant garnet granulites and eclogitic

rocks both increase following Birch's law [e.g., *Sobolev and Babeyko*, 1994]. Therefore our approach focusing on gabbroic assemblages is probably sufficient for igneous lower crust in general. This fractionation modeling also provides theoretical estimates for the temperature and pressure derivatives of velocity and density (J. Korenaga et al., submitted manuscript, 2000). Using these derivatives, a conversion law defined at specific temperature and pressure can be used to calculate in situ density ρ from in situ velocity V as

$$V_r(p_r, T_r) = V(p, T) + \frac{\partial V}{\partial p}(p_r - p) + \frac{\partial V}{\partial T}(T_r - T),$$

$$\rho_r(p_r, T_r) = f[V_r(p_r, T_r)], \qquad (1)$$

$$\rho(p, T) = \rho_r(p_r, T_r) + \frac{\partial \rho}{\partial p}(p - p_r) + \frac{\partial \rho}{\partial T}(T - T_r),$$

where p_r and T_r are reference pressure and temperature (1000 MPa and 25°C), respectively, at which velocity to density conversion, $\rho = f(V)$, is defined, and p and T are in situ pressure and temperature, respectively.

Using the above conversion laws for the four subdomains, i.e., the sedimentary layer, the continental crust, the upper crust, and the lower crust, a gravity anomaly was calculated based on the P wave velocity model for transect 2. Although pressure and temperature derivatives are not constant and have a roughly linear dependence on velocity and density (e.g., J. Korenaga et al., submitted manuscript, 2000), the calculation of gravity anomalies using average derivatives for expected ranges of velocity and density is sufficiently accurate, with an error of <0.5 mGal. The pressure and temperature derivatives that we used for velocity are 0.2×10^{-3} km s^{-1} MPa^{-1} and -0.4×10^{-3} km s^{-1} °C^{-1}, respectively, and those for density are 0.01×10^{-3} Mg m^{-3} MPa^{-1} and -0.03×10^{-3} Mg m^{-3} °C^{-1}, respectively. Temperature at seafloor is set as 0°C, and the geotherm is calculated with a vertical thermal gradient of 20°C km^{-1}, which is appropriate for 40- to 60-m.y.-old lithosphere [e.g., *Parsons and Sclater*, 1977].

To propagate the uncertainty of the velocity model to that of a predicted gravity anomaly, we utilize 100 Monte Carlo ensembles of the velocity model obtained by *Korenaga et al.* [2000]. Because any model parameter in a tomographic model is correlated with other parameters to some extent, the model covariance is fundamental to evaluate error propagation for averaged quantities such as the gravity anomaly. In particular, the uncertainty of the lower crustal velocity is expected to negatively correlate with the uncertainty of Moho depth because reflection travel times are the major constraint on the lower crustal structure. Therefore the uncertainty of the corresponding gravity anomaly correctly estimated using the model covariance can be smaller than that estimated with the model variance only. Though the explicit expression of the full model covariance matrix and its use for error propagation are computationally intractable, by repeating the same procedure of gravity calculation for each Monte Carlo ensemble and by taking the statistics of the resultant gravity anomalies, we can correctly incorporate the covariance of the velocity model into the uncertainty of the predicted gravity. Predicted gravity anomalies and densities obtained by this procedure are shown in Figure 4. To separate the effects of pressure and temperature corrections, two more anomalies are also shown in Figure 4a; the corrections for velocity, which has a much larger effect than those for density, result in a ~30 mGal increase at most compared with the case of no correction. The calculated gravity anomaly, however, still significantly
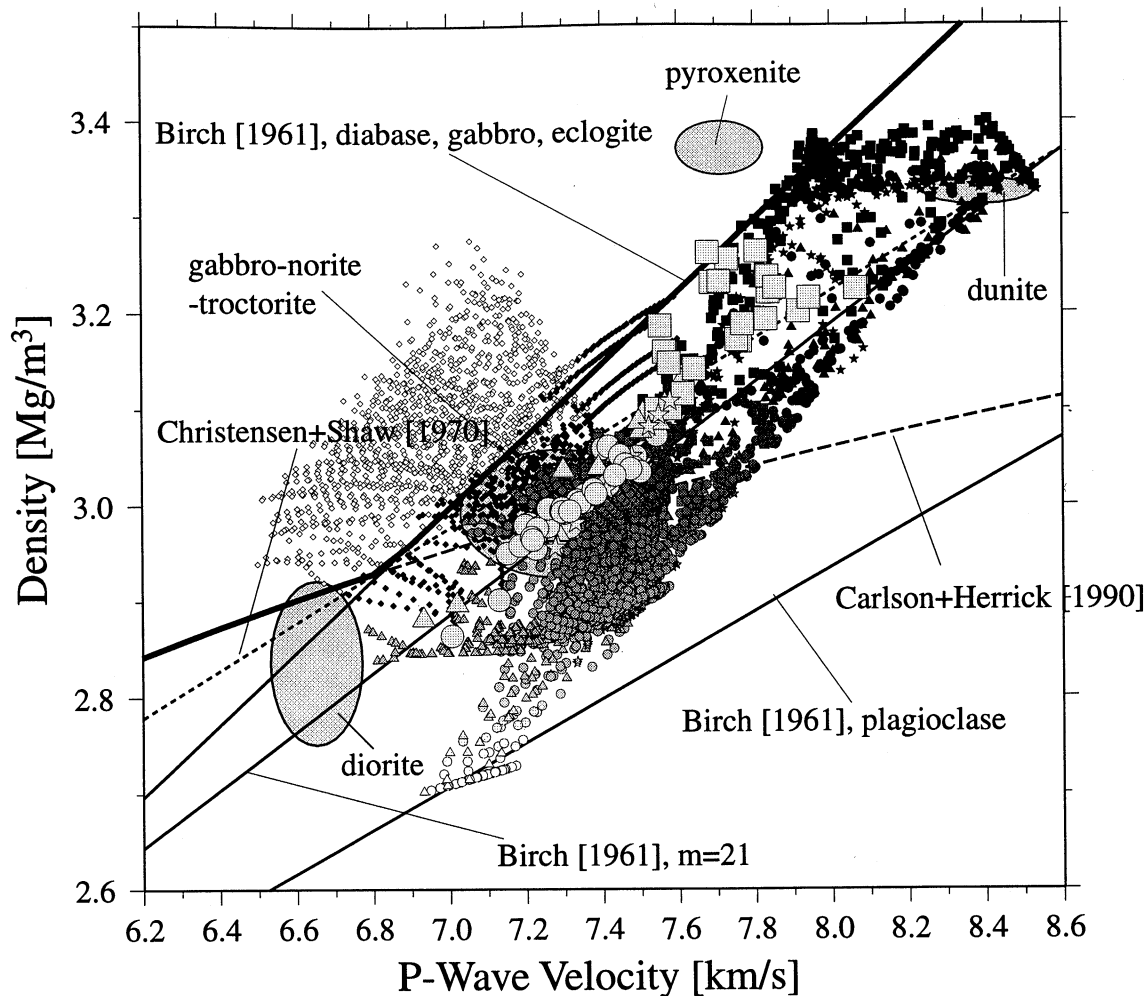
Figure 3. Covariation of P wave velocity and density of mafic and ultramafic rocks at 1000 MPa and 25°C. Large symbols denote values based on the CIPW norm calculation of mantle primary melts (circles [*Kinzler and Grove*, 1992,1993; *Kinzler*, 1997], triangles [*Hirose and Kushiro*, 1993], stars [*Baker and Stolper*, 1994], and squares [*Walter*, 1998]), and small symbols denote values of fractionated crystal assemblages based on fractional crystallization modeling at 100, 200, 400, and 800 MPa (see J. Korenaga et al. (submitted manuscript, 2000) for details). Velocity-density relationship adopted in this study is shown as thick solid line (Birch's law for diabase, gabbro, and eclogite). Also plotted are velocity and density of residual liquid compositions (solid diamonds for solid fractions <0.5, and open diamonds for solid fractions >0.5). Though density for residual liquids at late fractionation stages exceeds the adopted conversion law because of high FeO content, its contribution to lower crust is minimal, considering its small volume proportion. Ellipses denote laboratory data for diorite, gabbro-norite-troctolite, pyroxenite, and dunite, reported by *Christensen and Mooney* [1995]. Three solid lines are taken from *Birch* [1961] for plagioclase, rocks with mean atomic weight of ~21, and diabase-gabbro-eclogite. Dashed and dotted lines are for normal oceanic crust based on ODP/DSDP core data [*Carlson and Herrick*, 1990] and on samples dredged from the Mid-Atlantic Ridge [*Christensen and Shaw*, 1970].

underpredicts the observed anomaly by ~70 mGal over the continental shelf.

3. Possible Origins of the Margin Gravity High

Section 2 demonstrates that the seismic velocity model cannot explain the margin gravity high with the adopted velocity-density conversion. Though a constant mantle density assumed in our gravity calculation may be a source of this discrepancy, we will show that a possible density variation in our mantle section has only a small contribution if constant source mantle composition is assumed throughout continental rifting and subsequent seafloor spreading. Remaining possibilities are then limited to crustal

contributions: (1) the true velocity structure may be somehow very different from our velocity model and/or (2) the standard velocity-density conversion may not apply to our transect. We will test these possibilities in turn by quantifying a source density anomaly using the inversion of gravity anomalies and by revisiting travel time tomography with the additional constraint of observed gravity anomalies.

3.1. Mantle Contributions

A mantle Bouguer anomaly (MBA) is calculated by subtracting the predicted gravity anomaly based on the density model shown in Figure 4b from the observed free-air anomaly (Figure 5a). The nonzero MBA indicates a density variation in
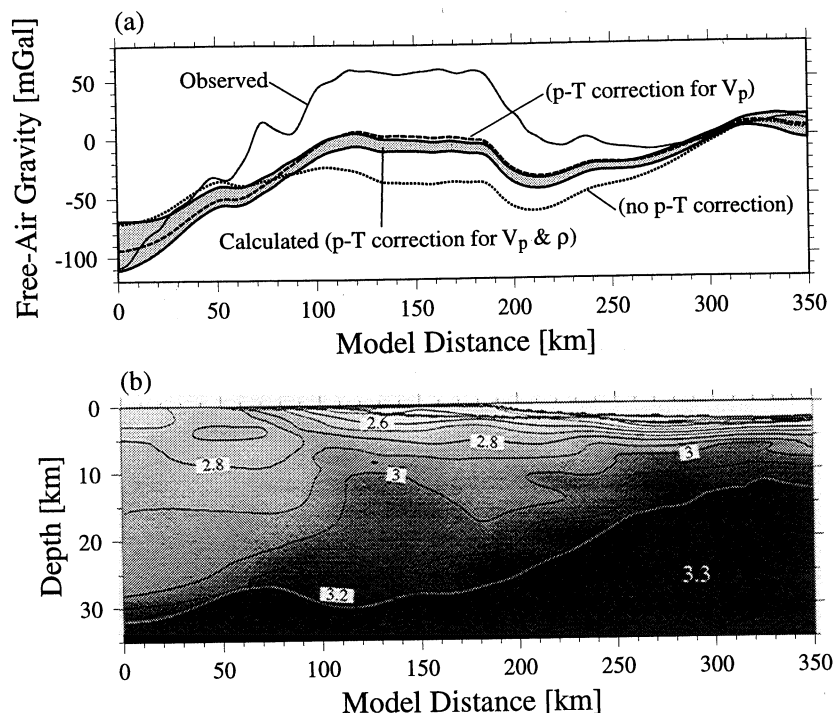
Figure 4. (a) Predicted free-air gravity anomaly (±1σ) based on (b) the density model, plotted with observed free-air gravity anomaly. Pressure and temperature corrections are applied to both velocity and density conversions. Also shown are gravity anomalies with no pressure and temperature corrections (dotted) and with pressure and temperature corrections for velocity conversion only (dashed).

the mantle section or an error in the crustal density model or both. Though the separation of the MBA into mantle and crustal components is nonunique, we can place a bound on the mantle contribution by modeling a plausible thermal and depletion history for the mantle underlying the igneous crust. We first estimated the order of required density variations in the mantle to explain the MBA, using an inversion technique described in Appendix A. The resultant 1-D density variations for the mantle section, with different maximum depth extents for the anomalous region, are shown in Figure 5b. The amplitude of the mantle density anomaly varies from 0.04 to 0.06 Mg m^{-3} for the range of the maximum depth, corresponding to a temperature variation of 400-600°C or a compositional variation of 2 to 3% in the Mg number [*Jordan*, 1988]. Whereas this degree of temperature variation does not seem reasonable for our mantle section, the alternative compositional variation is comparable to that which has been suggested by *Korenaga and Kelemen* [2000] for the North Atlantic igneous province. The major element heterogeneity of the source mantle in this province is, however, yet to be further confirmed with additional geochemical data, and given the present paucity of available data for the study of major-element source heterogeneity, we consider it too premature to conclude that the observed MBA can be ascribed solely to the compositional heterogeneity in the mantle. While keeping this type of mantle contribution as an alternative explanation, we need to investigate the possibility of crustal contribution to the MBA. For this purpose, it is important to first limit how much of the MBA can be explained by a possible density variation in the mantle, without invoking the compositional heterogeneity in the source mantle.

The formation age of the igneous crust varies from 61 Ma to 43 Ma along the transect, and older lithospheric mantle beneath

the thicker igneous crust would be colder and thus denser. The mantle thermal structure is calculated using the plate cooling model of *McKenzie* [1978]; a geotherm is obtained as a function of time by

$$\frac{T(t,z)}{T_a} = \frac{z}{a} + \frac{2}{\pi^2}\sum_{n=1}^{\infty}\frac{(-1)^{n+1}a}{n^2b}\sin\left(\frac{n\pi b}{a}\right)$$
$$\cdot\sin n\pi\left(1-\frac{z}{a}\right)\exp\left(-\frac{n^2\pi^2\kappa t}{a^2}\right), \qquad (2)$$

where T_a, a, b, and κ are asthenospheric temperature, plate thickness, the initial thickness of a lithospheric lid, and thermal diffusivity, respectively. We use the observed crustal thickness for the initial lid thickness and set the thermal diffusivity of mantle peridotite as 10^{-6} m^2 s^{-1}. The 2-D thermal structure is converted to a mantle density model using the thermal expansion coefficient of 3×10^{-5} K^{-1} and the adiabatic compressibility of 8×10^{-3} GPa^{-1} [*Turcotte and Schubert*, 1982]. A density difference due to an age difference is mostly confined to depths <100 km. Although the density contrast can be slightly increased by increasing the asthenospheric temperature and the plate thickness, those effects are trivial for the already cold lithosphere with the age difference of <20 m.y. (Figure 6a). For simplicity, we first model the mantle beneath the continental crust as 60-m.y.-old oceanic lithosphere in this and succeeding examples. However, this simplified treatment results in an positive gravity anomaly increasing toward the landward end of the transect (Figure 6a, curves A-C), which is incompatible with the overall trend of the MBA. The assumption that the subcontinental mantle is the same as that beneath the new, oceanic crust offshore is probably inappropriate because the Greenland continental crust is of the Archean age and the Greenland mantle lithosphere is probably
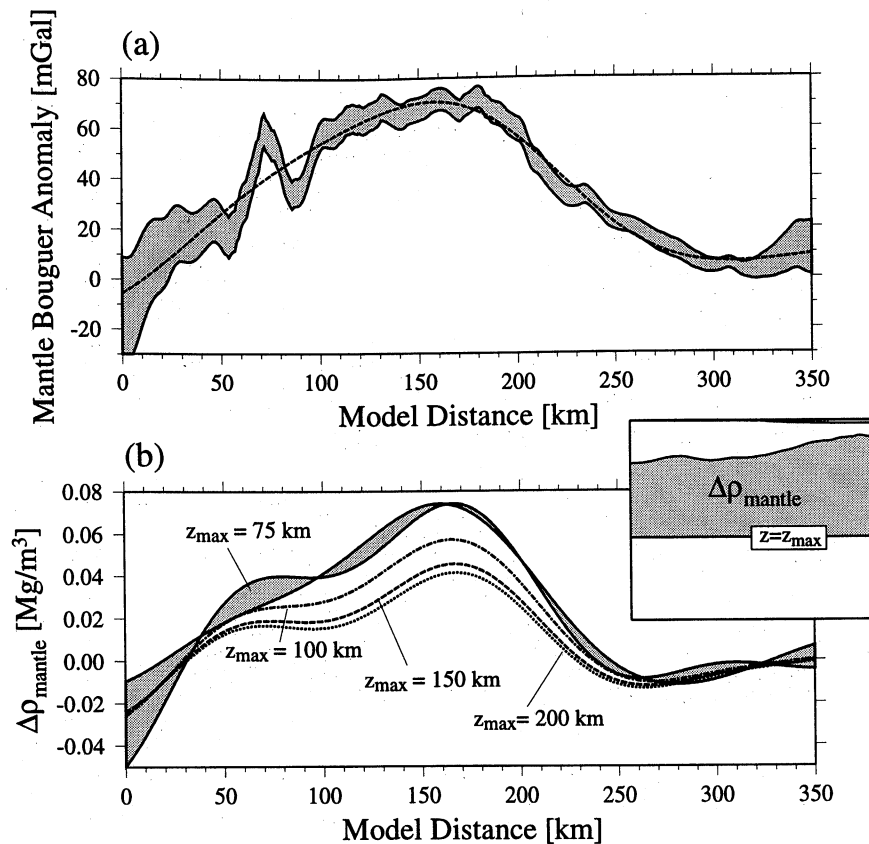
Figure 5. (a) Mantle Bouguer anomaly based on crustal density model shown in Figure 4b. Dashed line denotes fitted gravity anomaly obtained in the inversion for mantle density anomaly. Virtually identical fits are obtained for different maximum compensation depths. (b) Mantle density anomalies for different maximum compensation depths (solid, 75 km; dash-dotted, 100 km; dashed, 150 km; and dotted, 200 km). One standard deviation is shown for the case of maximum depth of 75 km. A low-pass filter used in this inversion is cosine-tapered with cut wavelength of 80 km and pass wavelength of 100 km.

highly depleted compared to the oceanic lithosphere [*Bernstein et al.*, 1998]. Considering its depleted nature, the continental lithosphere at model distances <50 km can be less dense than oceanic mantle despite its greater age and consequently lower temperature [e.g., *Jordan*, 1988]. To account for this effect, the required buoyancy is modeled to reduce predicted gravity at the landward end to zero (Figure 6a, curve A+). The amplitude of the resultant gravity anomaly due to mantle density anomaly is ~20 mGal.

Differentiation processes associated with continental rifting can significantly modify the mantle density structure, so that we need to include the effect of mantle depletion in addition to the temperature and pressure effects discussed above. We first used the mantle depletion model of *Klein and Langmuir* [1987]; the fertile plagioclase lherzolite and garnet-spinel lherzolite have densities of 3.27 and 3.34 Mg m^{-3}, respectively, at atmospheric pressure and 25°C, and the boundary between plagioclase and spinel lherzolite is set at 0.8 GPa. Igneous crust is generated by the passive upwelling of mantle, so thicker crust requires a higher degree of depletion of hotter asthenosphere, which results in more buoyant present-day mantle. A mantle density model predicted by this passive upwelling scenario has a gravity anomaly with a trend opposite to the trend of the observed MBA (Figure 6b). As suggested by the petrologic interpretation of the seismic velocity model of transect 2, active mantle upwelling

seems to have been significant during the formation of this continental margin, and the mantle potential temperature was probably almost constant despite the strong variation in crustal thickness [*Korenaga et al.*, 2000]. Therefore we next considered a mantle depletion model with an average degree of melting of 12% throughout the transect (Figure 6c). A positive amplitude is then recovered, and after correcting for the density of the continental lithosphere, the amplitude of the gravity anomaly is ~15 mGal (Figure 6c); the effect of mantle depletion only reduces the mantle contribution in the MBA.

The subcrustal fractionation of mantle melt to form ultramafic cumulates could also affect the bulk density of shallow mantle. Geochemical studies of the North Atlantic igneous province indicate an important role for high-pressure fractionation (8-15 kbar) during the ascent of magma through lithosphere [*Morrison et al.*, 1985; *Thompson et al.*, 1986; *Bernstein*, 1994; *Fram and Lesher*, 1997]. The effect of preexisting lithosphere might persist during continental rifting, so crystallization from primary melt might have started within the mantle lithosphere. At high pressures, crystallizing phases from basaltic liquids are generally olivine, then clinopyroxene, and then plagioclase [e.g., *Bender et al.*, 1978; *Presnall et al.*, 1978; *Grove et al.*, 1992; *Langmuir et al.*, 1992]. During olivine-only fractionation and olivine+clinopyroxene fractionation, the forsterite content of crystallizing olivine gradually decreases because of Fe-Mg
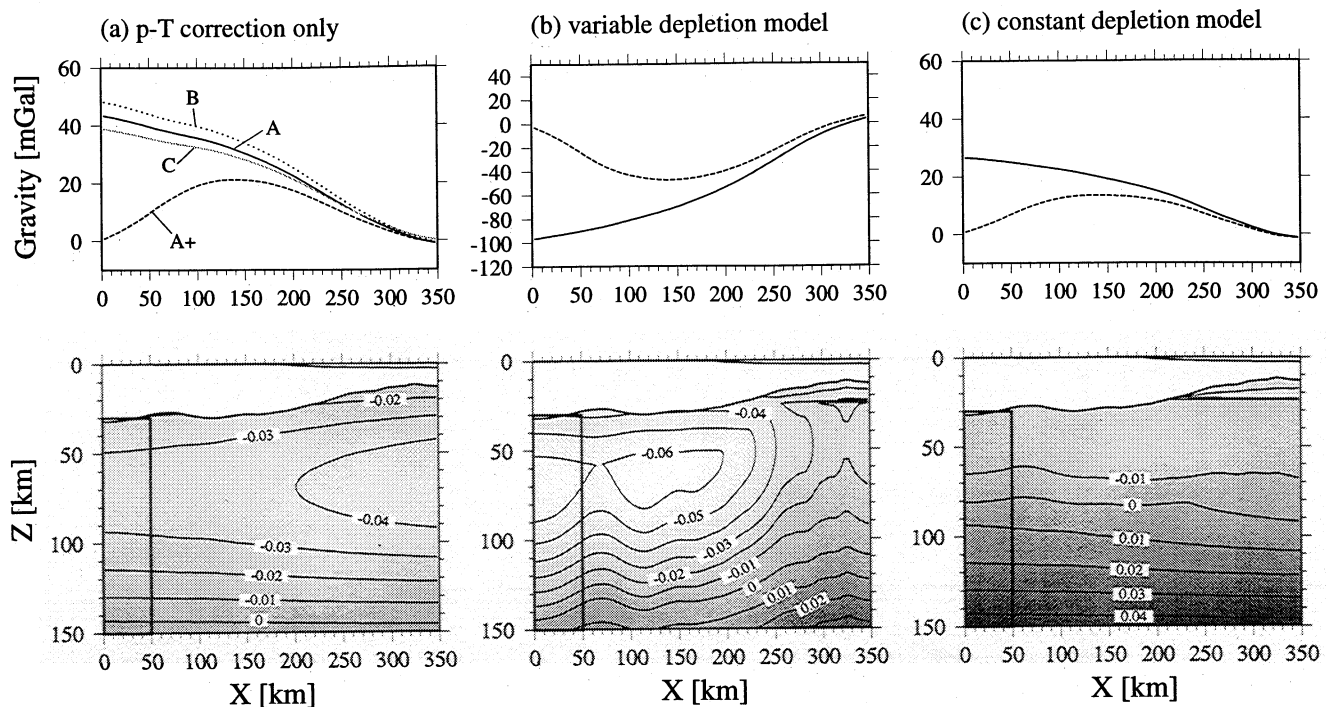
Figure 6. Three different models for (bottom) mantle density anomaly and (top) corresponding gravity anomalies. Mantle density anomaly is relative to 3.3 Mg m^{-3}, the constant value assumed in the other density models. (a) Mantle density anomaly from pressure and temperature effects only. Mantle thermal field is based on 1-D thermal evolution model. Curve A (solid), T_a=1350°C and a=200 km; curve B (dotted), T_a=1450°C and a=200 km; and curve C (gray), T_a=1350°C and a=125 km. Curve A+ (dashed) is obtained by adding negative density anomaly of 0.015 Mg m^{-3} for the region enclosed by solid box (continental lithosphere). (b) Variable depletion model. In addition to temperature and pressure corrections, the effect of mantle depletion required to produce the observed crustal thickness based on passive mantle upwelling model is incorporated (solid). Asthenospheric temperature is varied accordingly, and plate thickness is held constant at 200 km. A positive density anomaly of 0.032 Mg m^{-3} is added to continental lithosphere to increase the landward end of gravity anomaly to zero (dashed). (c) Constant depletion model. Average degree of melting is held constant at 12% with plate thickness of 200 km (solid). A negative density anomaly of 0.009 Mg m^{-3} is added to continental lithosphere to reduce the landward end of gravity anomaly to zero (dashed).

partitioning between olivine and liquid [*Roeder and Emslie*, 1970] if fractionating liquid does not react with surrounding mantle. Relatively Fe-rich olivine cumulates at subcrustal levels could increase bulk mantle density. The density of crystal assemblages calculated in the fractionation modeling (Figure 3) is used to quantify this effect (Figure 7). The magnitude of the positive density anomaly depends on the initial liquid Mg number; a lower Mg number results in a shaper decrease in the forsterite content (Figure 7a). The overall impact on mantle density is limited by the appearance of the second crystallizing phase, and the resulting bulk density anomaly rarely exceeds 0.02 Mg m^{-3} (Figure 7b). For 30-km-thick crust, for example, as much as 20% subcrustal fractionation would merely result in a 7.5-km-thick layer with a density anomaly of 0.02 Mg m^{-3}. This is an order of magnitude smaller than the mantle density anomaly required to explain the MBA (Figure 5b), indicating that this effect is only of minor significance in this study.

3.2. Crustal Contributions

3.2.1. Crustal density anomalies. Having explored a reasonable range of thermal and depletion history for our mantle section, we can conclude that if there is no major element heterogeneity in the source mantle, the mantle contribution to the

observed MBA is ~20 mGal at largest and that the rest of the MBA must originate in the crust. Given the uncertainty in our modeling of mantle origin gravity anomalies, we will hereinafter consider three different residual gravity anomalies including the original MBA to investigate the crustal contribution (Figure 8); the residual anomalies are inverted for density anomalies in the whole crust, the lower crust, and the upper crust (Figure 9). An inversion fit similar to the one shown in Figure 5a was obtained for all inversions. Note that these inversion results depend on the choice of reference density structure in the gravity calculation. If we choose to define the reference model to match a predicted anomaly over the continental shelf with the observed anomaly, for example, the resultant MBA would be all negative except over the shelf, and the required variation in crustal density would nearly double because the largest residual anomaly would now correspond to the thinnest crust. Since the seaward section of the transect is best resolved in the seismic velocity model and is similar to the normal oceanic crust, which has tightly constrained velocity-density systematics, it can be confidently treated as the reference for our gravity modeling.

The whole crustal density anomaly has an amplitude of 0.06-0.08 Mg m^{-3} (Figure 9a). A systematic error of this degree in our upper crustal density model could be acceptable because the velocity to density conversion law of *Carlson and Herrick* [1990]
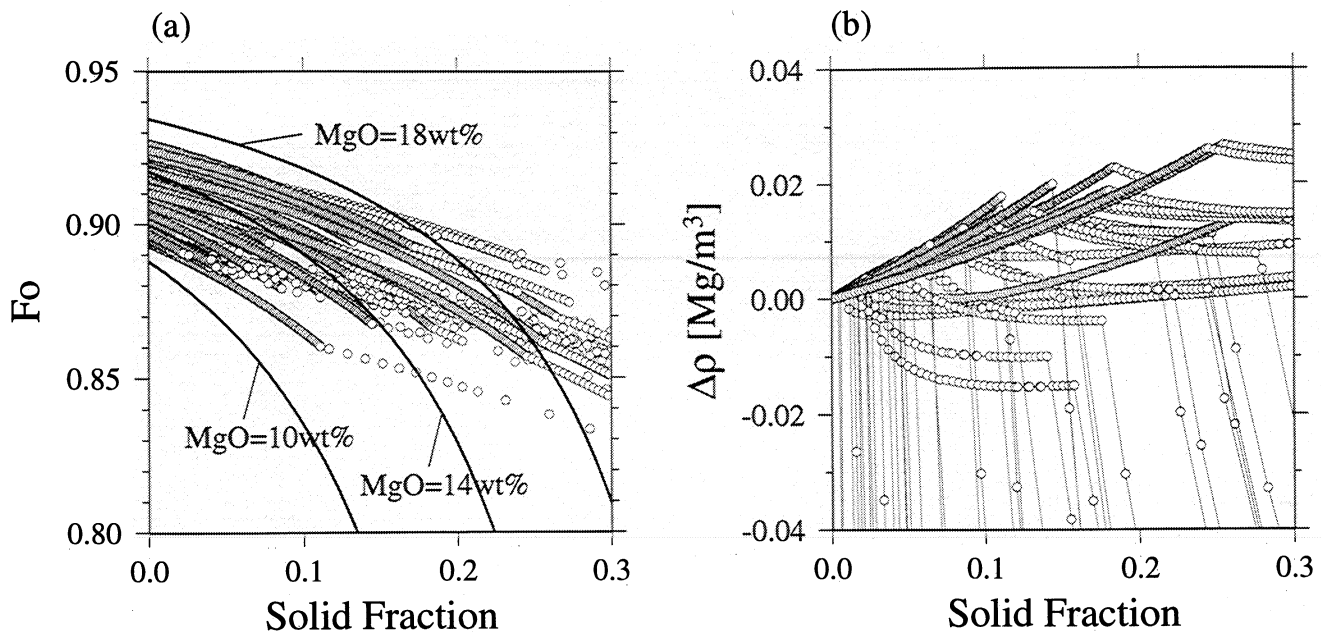
(a)

(b)

Figure 7. Summary of high-pressure fractionation in terms of olivine composition and density anomaly based on fractional crystallization modeling at 800 MPa. Densities are calculated at 800 MPa and 480°C (deep Moho condition). (a) The olivine composition of the incremental crystal assemblage as a function of total solid fraction. Also shown are hypothetical olivine fractionation paths starting from initial liquids with 7.5 FeO wt % and 10, 14, and 18 MgO wt %, using olivine-liquid Fe-Mg exchange coefficient of 0.30. Because of addition of clinopyroxene and/or plagioclase in fractionating assemblage at a solid fraction >0.1, decrease in the forsterite content is more reduced in more realistic fractionation paths. (b) Increase in the density of cumulative fractionated assemblage with respect to the initial olivine density as a function of solid fraction. Because of appearance of clinopyroxene and plagioclase, the effect of the low forsterite content on the bulk density is limited up to ~0.025 Mg m^{-3}.

has a similar uncertainty. Since the conversion law that we adopt for the lower crust provides the greatest possible density for a given velocity, however, this density anomaly must be attributed to a systematic error of >0.16-0.21 km s^{-1} in the lower crustal velocity, which substantially exceeds the absolute error of 0.05-0.10 km s^{-1} estimated by the nonlinear Monte Carlo analysis [*Korenaga et al.*, 2000]. In addition, the average crustal velocity has a smaller error of ~0.03 km s^{-1} because of the negative correlation of parameter uncertainty, further reducing the

possibility of such a large systematic error in the lower crustal velocity.

Restricting the density anomaly to the lower crust causes an even larger density anomaly (Figure 9b), so we are unable to explain this density anomaly for the same reason. The upper crustal density anomaly naturally has a much greater amplitude (Figure 9c), and the anomaly of ~0.2 Mg m^{-3} cannot be explained by either the uncertainty of the conversion law or an error in the upper crustal velocity. The upper crust is the best constrained part
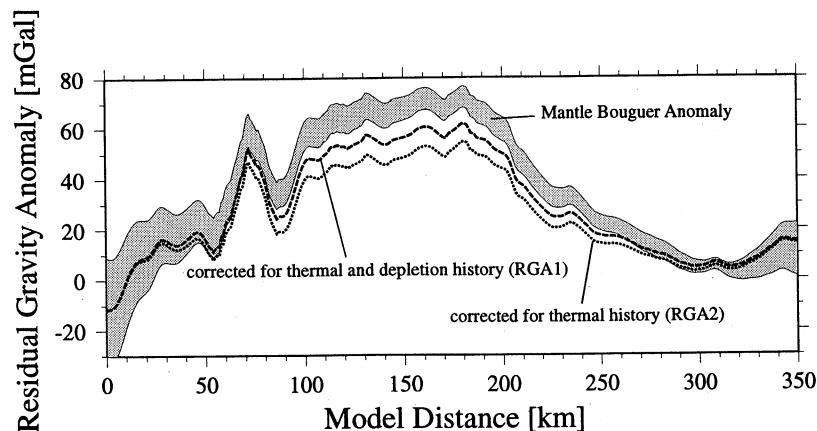

Figure 8. Three candidates for residual gravity anomalies. MBA (solid with one standard deviation) is original mantle Bouguer anomaly as shown in Figure 5a, RGA1 (dashed) is corrected for the mantle density model shown in Figure 6c, and RGA2 (dotted) is corrected for the mantle density model shown in Figure 6a. RGA1 is our preferred choice since it incorporates the most likely thermal and depletion history of the mantle beneath the transect. Standard deviations for RGA1 and RGA2 are the same as for MBA and are omitted for clarity.
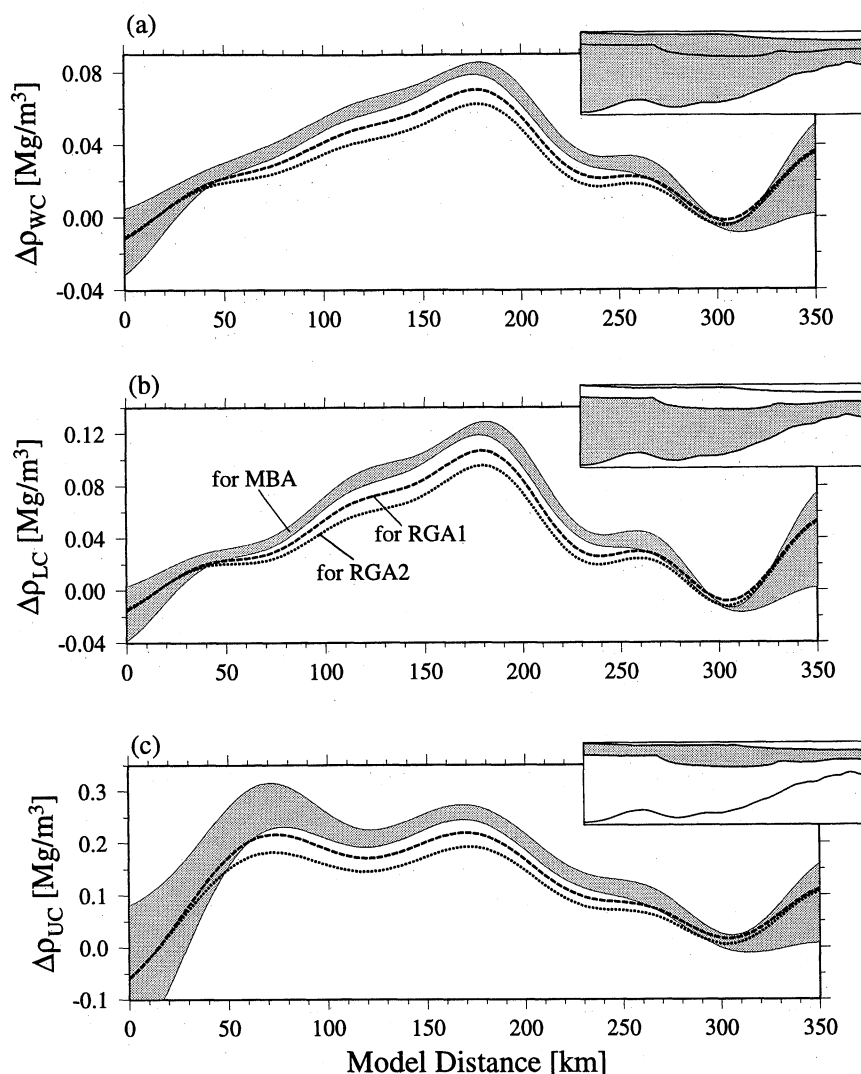
Figure 9. Results of inversion for crustal density anomalies. Solid lines show the density anomalies for the gravity anomaly input of MBA, dashed for RGA1, and dotted for RGA2. For clarity, one standard deviation is shown only for MBA results. (a) Whole crustal density anomalies, (b) lower crustal density anomalies, and (c) upper crustal density anomalies. Note that we slightly modified the upper/lower crust boundary from that shown in Figure 1c to avoid zero thickness in the upper crust for the onshore region. A low-pass filter used in this inversion is cosine tapered with cut wavelength of 50 km and pass wavelength of 70 km. All crustal density anomalies become zero around km 300, from which the reference density model was taken. Large uncertainty toward the seaward end originates in the uncertainty of the original velocity model, which is amplified by inverting gravity anomalies for a thin crustal layer.

of the tomographic model owing to the dense coverage of refraction rays [*Korenaga et al.*, 2000]. Although there is a possibility of having a completely different conversion law for the upper crust, as we will discuss in section 3.2.3, we would like to first make a conservative review of our previous estimate of the uncertainty of the seismic velocity model and reexamine its reliability. One may argue that for example, the number of ensembles used in our Monte Carlo analysis is not sufficiently large to provide the definitive estimate of the a posteriori covariance. This type of criticism is always valid for the Monte Carlo method unless the number of ensembles is extremely large, which we regard as an unrealistic ideal for our large-scale tomography, so we must seek an alternative, independent check on our uncertainty analysis. Since the majority of the lower crust is constrained only by reflection travel times, we think it

beneficial to revisit the tomography problem by jointly inverting seismic travel times and gravity anomalies. The virtue of this joint inversion is that the exploration of the model space is biased to some subspace that can explain an input gravity anomaly, thereby supplementing the possibly limited search of the model space by Monte Carlo randomization.

3.2.2. Travel time tomography revisited. The formulation of the joint inversion of seismic travel times and gravity anomalies is given in Appendix B. A starting model is the velocity model shown in Figure 1c, and correlation length functions for velocity and depth nodes are the same as those of *Korenaga et al.* [2000]. Depth-kernel weighting is set as unity for all inversions. The slowness derivatives of density are based on the velocity-density conversion laws as chosen above except for the sedimentary layer, for which we assign zero sensitivity. The travel time data
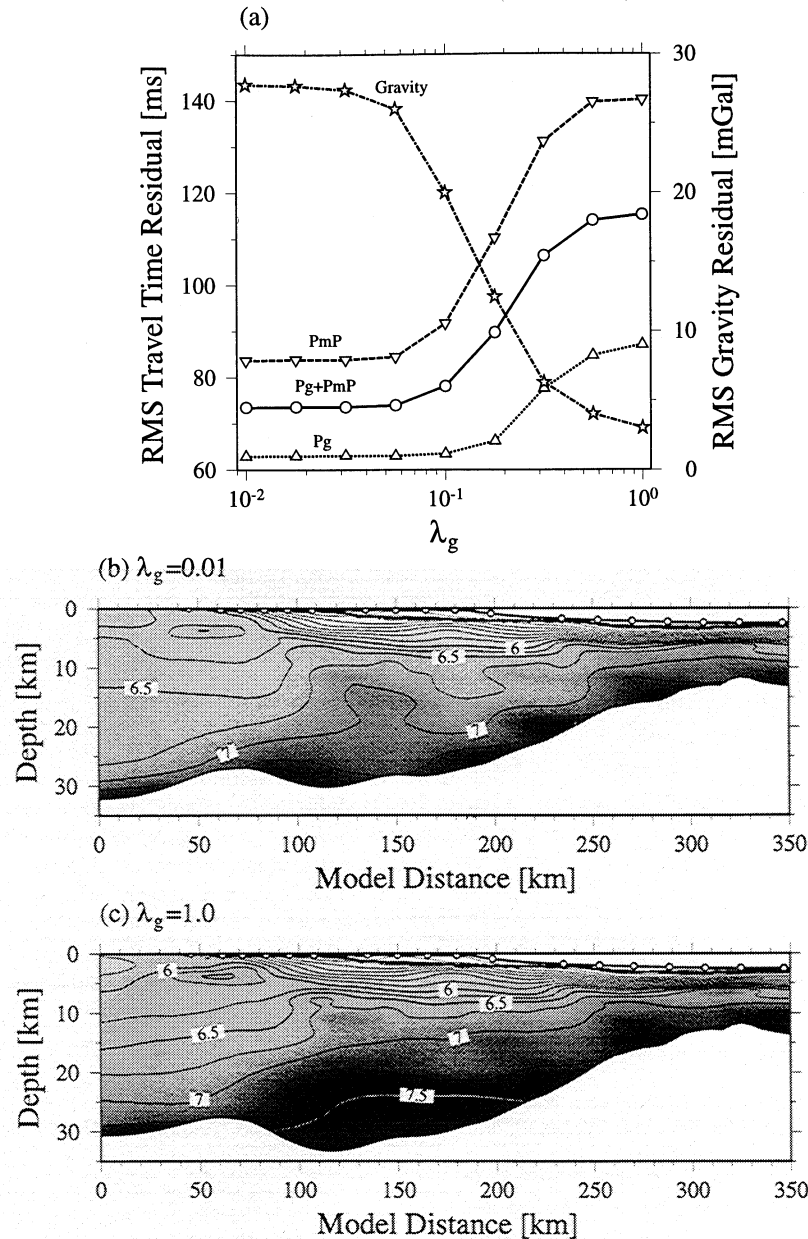
Figure 10. Result of joint inversion of seismic travel times and gravity anomalies. (a) RMS travel time residuals for *Pg* (triangle), *PmP* (inverse triangle), and both (circle), and RMS gravity residual (star) are plotted as a function of the gravity weighting parameter λ_g. (b) Final velocity model obtained with λ_g of 0.01. (c) Final velocity model obtained with λ_g of 1.0. Open circles denote the location of onshore/offshore seismometers deployed during the SIGMA experiment.

consist of 2318 *Pg* and 2078 *PmP* picks from 25 instruments, and the gravity anomaly data consist of 76 data points sampled from the observed free-air gravity anomaly with a 5-km interval. With the smoothing weights fixed, the gravity-kernel weighting parameter λ_g is varied from 0.01 to 1. For each choice of λ_g the inversion converged within five iterations. The results are summarized in Figure 10a. There is almost no reduction in a root-mean-square (RMS) gravity residual with small λ_g, and the corresponding final velocity model (Figure 10b) is virtually identical to the starting model. The RMS gravity residual starts to decrease drastically around λ_g of 0.1 and reaches ~3 mGal for the largest λ_g. The long-wavelength variations in the observed gravity anomaly are completely fitted using a density model

corresponding to the velocity model shown in Figure 10c, and the small residual is mostly due to the short-wavelength feature observed at model distances of km 60-90 (Figure 1b). This final velocity model has a high-velocity root (~7.5 km s⁻¹) in the lowermost crust at km 80-230. There is, however, a strong trade-off between the travel time constraint and the gravity constraint; while the RMS gravity residual reduces by increasing the gravity-kernel weighting, the travel time fits significantly deteriorate, especially for the *PmP* phase (Figure 10a).

This exercise demonstrates that there is no hidden model space that we might have missed in our previous Monte Carlo uncertainty analysis; if there were such model space, we should observe no change in the travel time fits, while gravity fits are
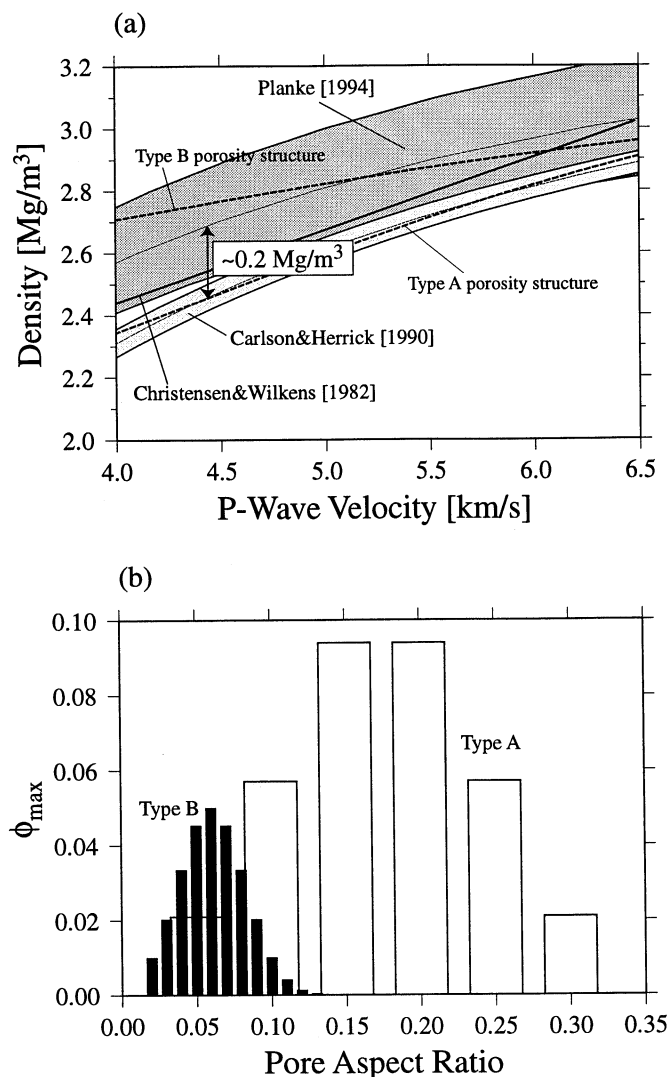
Figure 11. (a) Relationship of P wave velocity with density of mafic rocks established for upper oceanic crust [*Carlson and Herrick*, 1990], Iceland plateau basalt sequences [*Christensen and Wilkens*, 1982], and seaward dipping reflector sequences at the Vøring margin [*Planke*, 1994]. Also shown as dashed are results of forward modeling of velocity-density systematics using the pore aspect ratio spectrum shown in Figure 11b. We first calculated effective elastic moduli of dry porous rock with the formula of *Kuster and Toksöz* [1974] and then applied the Gassmann low-frequency relations to obtain effective moduli for fluid saturated porous rock [e.g., *Mavko et al.*, 1998]. Elastic moduli for basalt and seawater are taken from *Wilkens et al.* [1991]. (b) Histogram of pore aspect ratios for type A and type B.

improved. Although the joint inversion does place the needed high-velocity material at the least resolved part of the velocity model, the travel time constraint is largely violated, so that the final velocity model such as shown in Figure 10c can be rejected. One may note that a part of the gravity misfit can be explained without strongly violating the travel time data, such as the case of setting λ_g to 0.1 (Figure 10a). Considering that the densest possible conversion was used for the lower crust, however, it is very unlikely that we can accept a denser lower-crustal model than derived by the original velocity model. Therefore the residual gravity anomaly cannot be attributed to the lower crust

despite the fact that it has the largest volume contribution and the largest model uncertainty.

3.2.3. Is upper crust denser? The upper crust of transect 2 constitutes ~30% of the whole crustal volume, and its velocity structure has an uncertainty of ~0.04 km s^{-1} [*Korenaga et al.*, 2000]. The density conversion law of *Carlson and Herrick* [1990] is well constrained with one standard deviation of 0.07 Mg m^{-3}. The upper crustal density anomaly of ~0.2 Mg m^{-3} required to explain the residual gravity anomaly (Figure 9c) therefore seems difficult to reconcile with the seismic data. The velocity-density systematics for the upper oceanic crust is largely controlled by porosity, and Carlson and Herrick's empirical law is based on a number of laboratory measurements of samples collected from the oceanic crust and ophiolites [*Carlson and Raskin*, 1984, and references therein]. We note, however, that the velocity and density of lavas recovered from the ODP Site 642 (Vøring margin) and Site 917 (southeast Greenland margin) are systematically offset, despite large scatters, from Carlson and Herrick's law [*Planke*, 1994; *Planke and Cambray*, 1998] (Figure 11a). Though there are only two drilling sites that show this trend and the penetration depths into basaltic rocks are <1 km, this systematic offset of ~0.2 Mg m^{-3} in density or 1.0 km s^{-1} in velocity might be a fundamental difference between normal oceanic upper crust and the upper crust of North Atlantic continent-ocean transition zones. Volcanic passive margins are characterized by the occurrence of seaward dipping reflectors, which resulted from vigorous subaerial eruptions [e.g., *Hinz*, 1981]. Multichannel seismic reflection data on our transect show several seaward dipping reflectors within the transition zone upper crust, and the basement high located around km 240 likely marks a transition from subaerial eruption to submarine eruption [*Korenaga et al.*, 2000]. Most of the upper crustal density anomaly is confined to the thick transition zone upper crust (Figure 9c), suggesting that Planke's conversion law should be preferred for that part of the upper crust.

Several possibilities have been proposed for the difference between the two conversion laws for the igneous upper crust, including compositional effects, porosity structure, and the degree of alteration [*Planke*, 1994]. Plateau basalts tend to have lower Mg numbers than mid-ocean ridge basalts (MORBs), and the corresponding increase in the iron content may be a major reason to modify the velocity-density systematics (e.g., Figure 3). However, whereas Icelandic plateau basalts do indeed have higher grain densities [*Christensen and Wilkens*, 1982], reported grain densities for samples from the Greenland margin are virtually the same as that for average MORB [*Larsen et al.*, 1994; *Duncan et al.*, 1996], so it is unlikely that the systematic offset results from a difference in matrix density. Alternatively, subaerial lava emplacement could result in a different porosity structure, and we note that the velocity of porous rocks is highly sensitive to the spectrum of pore aspect ratios [e.g., *Wilkens et al.*, 1991]. Porosity structure is also affected by alteration, largely controlled by hydrothermal circulation and cooling history, which can substantially differ between plateau basalts and MORBs. Simple forward modeling was conducted to illustrate the effect of porosity structure (Figure 11); the spectra of pore aspect ratios are modeled to fit the overall trend of the two empirical conversion laws. The chosen spectra are, of course, arbitrary, in the sense that there are many other solutions to generate similar fits, but the potential of porosity structure in modifying velocity-density systematics is clear from this example.

The residual gravity anomaly of 40-60 mGal over the transition zone crust might therefore be due to a denser upper
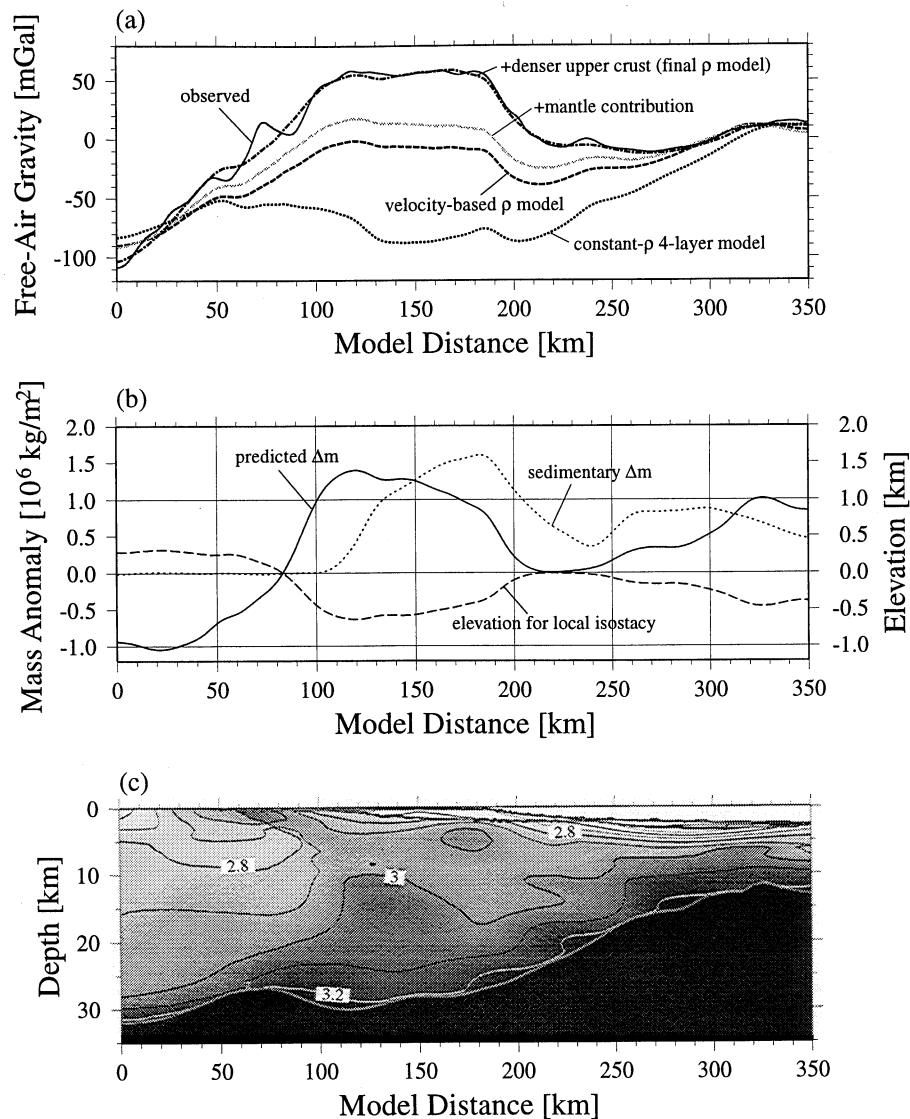
Figure 12. (a) Free-air gravity anomaly corresponding to the final density model shown in Figure 12c (dot-dashed) with observed anomaly (solid) and other preliminary predicted anomalies. (b) Mass anomaly for a 36-km-thick vertical column (from 1 km above the sea surface to 35 km deep) along the transect (solid) is plotted based on the final density model shown in Figure 12c. Hypothetical mass anomaly based on observed sedimentary load, $(\rho_{sediment}-\rho_{water}) H_{sediment}$, is shown as dotted. Also shown is elevation required to attain local isostatic equilibrium (dashed). (c) Final density model constructed by adding upper crustal density anomaly corresponding to RGA1 to the density model shown in Figure 4b. Cosine window is used to taper down the density anomaly toward the bottom boundary of the upper crust, and the density anomaly is then scaled up to conserve the total density anomaly.

crust, compared to the oceanic upper crust. Our preferred density model, incorporating this upper crustal density anomaly, is presented in Figure 12c. The corresponding gravity anomaly shows an excellent fit with observations, providing an independent check on the accuracy of our inversion method (Figure 12a). A mass anomaly based on the final density model is shown in Figure 12b, which is broadly comparable with a mass anomaly based on an observed sedimentary load, indicating that most of the current sedimentary load is not compensated by the underlying lithosphere. Since the thickest sediment column is only ~1.5 km, however, the transect is close to isostatic equilibrium; required surface elevations to attain local isostasy are <0.6 km along the transect (Figure 12b). The mode of

isostacy is of a mixed nature; the basement topography is balanced by both the crustal thickness variation (Airy-type isostacy) and the lateral density variation within the crust (Pratt-type isostacy).

4. Discussion and Conclusion

Gravity modeling has been a common exercise in studies of deep crustal structure [e.g., *Holbrook et al.*, 1994b; *Horsefield et al.*, 1994; *Chian et al.*, 1995; *Barton and White*, 1997; *Lizarralde and Holbrook*, 1997; *Reid and Jackson*, 1997; *Mjelde et al.*, 1998]; through the correlation between velocity and density, it can provide an independent check on a velocity model. There are,

however, several problems with this type of gravity modeling, which have often been overlooked in previous studies. Because the velocity-density systematics can have considerable uncertainty even for a single rock type due to compositional and porosity effects, and because a velocity model itself always has some estimation errors, constructing a density model that can satisfy a given gravity constraint could become arbitrary, considering the nonuniqueness of the derived density distribution. Being able to present a "consistent" pair of velocity and density models may only mean that an original velocity model is poorly constrained. We therefore need (1) to demonstrate how well a velocity model is constrained and (2) to translate its uncertainty into a density model. Velocity-depth ambiguity is inherent in the seismic constraint of reflection travel times, and the corresponding correlation between velocity and depth parameters should be used to provide a proper error estimate in gravity modeling. The Monte Carlo approach used in this study fulfills these requirements.

Uncertainty in velocity to density conversion is more problematic. For the continental crust, because of the variety of rock types that we can expect [e.g., *Christensen and Mooney*, 1995], rigorous error propagation does not seem to provide any useful outcome [*Barton*, 1986]. For the thick igneous and oceanic crust, however, we can reasonably assume a one-step crustal production from mantle melting, so that less ambiguous conversion is possible. This is especially true for the lower crustal section of thick igneous crust, which is very unlikely to be affected by seawater alteration. Even though there is still considerable scatter in the velocity-density relation of gabbroic rocks (Figure 3), a bounding approach such as our densest possible conversion is effective to systematically isolate density anomalies, together with the inversion method developed in this paper. Although the inversion of gravity anomalies is usually formulated to estimate the shape of a causative body [e.g., *Oldenburg*, 1974; *Granser*, 1987; *Guspi*, 1990], we showed that an alternative formulation to estimate density is particularly useful when reliable seismic information is available. Our success in this systematic approach is, however, somewhat fortuitous because the bounding approach largely depends on having well-constrained oceanic crust within the transect. On the basis of the presence of oceanic crust we were able to test various possibilities for the thicker transition zone crust. If we did not have such a reliable benchmark, the gravity modeling could have been almost meaningless, as lucidly demonstrated by *Barton* [1986].

Many passive continental margins show a gravity high similar to that in our transect. Whereas *Vogt et al.* [1998] proposed densified crust resulting from a gabbro-eclogite phase change as the most likely, general explanation for these gravity highs, such an explanation does not apply to our transect because the crustal velocity is too low to be interpreted as eclogite. Though we do not believe that there should necessarily be a single explanation for all passive margin gravity highs, the dense upper crust made of plateau basalts might be an important factor for gravity highs at volcanic margins worldwide. On the other hand, the thick, high-density lower crust has been the common explanation for gravity highs observed at volcanic rifted margins [e.g., *Morgan and Barton*, 1990]. The high-density lower crust seems to be supported by the corresponding high-velocity lower crust, but we note that this argument may deserve careful reexamination. Owing to limited experimental capability in the past, it is for only the last several years that we have been able to collect dense, high-quality seismic data and to confidently derive deep crustal

seismic structure. Deep crustal seismic studies in previous generations relied heavily on expanding-spread profiling, suffering from serious velocity-depth ambiguity for lower crustal structure (see discussion of J. Korenaga et al. (submitted manuscript, 2000)). The thick transition zone crust on our transect does not have notably high velocity; thus its density cannot be high enough to explain the gravity high. Instead, on the basis of a series of geophysical analyses in this paper we have suggested that the margin gravity high at the southeast Greenland margin originates in either (1) dense Fe-rich shallow mantle situated beneath the thick transition zone crust or (2) dense (in terms of conventional velocity-density conversion laws) upper crust in the transition zone. The geochemical study of the North Atlantic igneous province seems to favor the first explanation, while the physical properties of flood basalts derived from recent drilling legs seem to support the second. The continent-ocean transition zone is >100 km long, so the wavelength of the MBA is not particularly helpful to estimate the source depth. While it is difficult to decide which source is more preferable, we have demonstrated that the commonly employed lower crustal origin is not plausible at least for our data and that the upper crustal and mantle origins are worth more attention than previously given.

Appendix A: Inversion of Gravity Anomalies in the Presence of Upper and Bottom Topography

A 2-D gravity anomaly g_z caused by a 1-D density variation $\rho(x)$ bounded by $z=z_1(x)$ and $z=z_2(x)$ (Figure A1) may be expressed in the Fourier domain as [*Parker*, 1972]

$$F[g_z] = -2\pi G \exp(|k|z_0)$$
$$\cdot \sum_{n=1}^{\infty} \frac{(-|k|)^{n-1}}{n!} F[\rho(z_1^n - z_2^n)], \qquad (A1)$$

where $F[]$ denotes the 1-D Fourier transform with respect to the horizontal coordinate and G, z_0, and k are the universal gravity constant, the vertical coordinate of an observation plane ($z_0 < \min(z_1)$), and the horizontal wavenumber, respectively. A restriction to constant thickness is usually applied to separate the $F[\rho]$ term from other higher-order terms with topography variations and to construct an iterative inversion formula for the density variation [e.g., *Parker and Huestis*, 1974]. This limitation to constant layer thickness is only superficial, and an extension to variable thickness is straightforward. Noting that the 1-D density
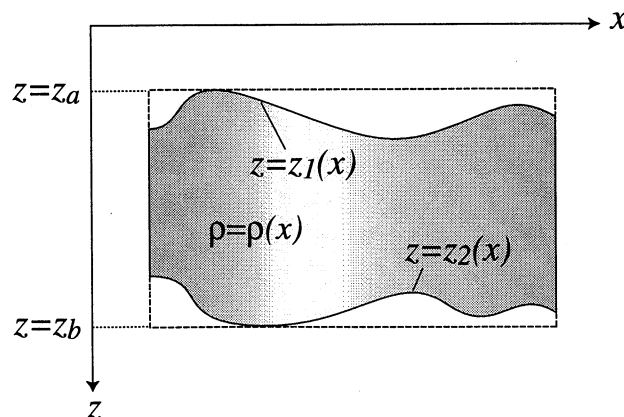

Figure A1. Schematic diagram showing the 2-D model geometry for the inversion of gravity anomalies in the presence of upper and bottom topography.

variation between the two boundaries can be also expressed as a layer of constant thickness and two topographic corrections, (A1) may be rewritten as

$$\frac{F[g_z]}{2\pi G e^{|k|z_0}} = \frac{1}{|k|}(e^{-|k|z_a} - e^{-|k|z_b})F[\rho] + \sum_{n=1}^{\infty}\frac{(-|k|)^{n-1}}{n!}$$
$$\cdot\{e^{-|k|z_a}F[\rho(z_1 - z_a)^n] - e^{-|k|z_b}F[\rho(z_2 - z_b)^n]\}, \quad (A2)$$

where $z_a = \min(z_1)$ and $z_b = \max(z_2)$. Since the convergence of the infinite series summation is fastest when a reference plane is located between the top and bottom boundaries [Parker, 1972], the more numerically efficient form of (A2) may be expressed as

$$\frac{F[g_z]}{2\pi G e^{|k|z_0}} = \frac{1}{|k|}(e^{-|k|z_a} - e^{-|k|z_b})F[\rho] + \sum_{n=1}^{\infty}\frac{(-|k|)^{n-1}}{n!}$$
$$\cdot\{e^{-|k|z_{r1}}F[\rho((z_a - z_{r1})^n - (z_1 - z_{r1})^n)]$$
$$+e^{-|k|z_{r2}}F[\rho((z_2 - z_{r2})^n - (z_b - z_{r2})^n)]\}, \quad (A3)$$

where $z_{r1} = (z_a + \max(z_1))/2$ and $z_{r2} = (z_b + \min(z_2))/2$. An iterative inversion formula for the density variation is thus obtained as

$$F[\rho] = \frac{|k|}{e^{-|k|z_a} - e^{-|k|z_b}}\left(\frac{F[g_z]}{2\pi G e^{|k|z_0}} - \sum_{n=1}^{\infty}\frac{(-|k|)^{n-1}}{n!}\right.$$
$$\cdot\{e^{-|k|z_{r1}}F[\rho((z_a - z_{r1})^n - (z_1 - z_{r1})^n)]$$
$$\left.+e^{-|k|z_{r2}}F[\rho((z_2 - z_{r2})^n - (z_b - z_{r2})^n)]\}\right). \quad (A4)$$

Note that, for $k=0$, the term $|k|/(e^{-|k|z_a} - e^{-|k|z_b})$ reduces to the reciprocal of the constant layer thickness, $1/(z_b - z_a)$. An annihilator can be constructed by setting $F[g_z] = 0$ and using $\delta(k)$ as an initial guess for $F[\rho]$. Because this inversion is essentially a downward continuation, proper low-pass filtering must be applied at each iteration to avoid the divergence of high wavenumber components.

Appendix B: Joint Inversion of Seismic Travel Times and Gravity Anomalies

Following the notation adopted by Korenaga et al. [2000], a linearized inverse equation for slowness and depth perturbations that are constrained by seismic travel times and gravity anomalies may be expressed as

$$\begin{bmatrix} \mathbf{d}_t \\ \lambda_g\mathbf{d}_g \\ 0 \\ 0 \\ 0 \end{bmatrix} = \begin{bmatrix} \mathbf{G}_v & w\mathbf{G}_d \\ \lambda_g\mathbf{F}_v & \lambda_g w\mathbf{F}_d \\ \lambda_v\mathbf{L}_{Hv} & 0 \\ \lambda_v\mathbf{L}_{Vv} & 0 \\ 0 & \lambda_d w\mathbf{L}_d \end{bmatrix}\begin{bmatrix} \delta\mathbf{m}_v \\ \frac{1}{w}\delta\mathbf{m}_d \end{bmatrix}, \quad (B1)$$

where $\mathbf{d}_t$ and $\mathbf{d}_g$ are residual travel times and residual gravity anomalies, respectively; $\mathbf{G}$ and $\mathbf{F}$ are Fréchet derivative matrices for travel times and gravity anomalies, respectively; the $\mathbf{L}$ matrices are for smoothing constraints; and the $\delta\mathbf{m}$ vectors are for model perturbations. The subscripts v and d denote
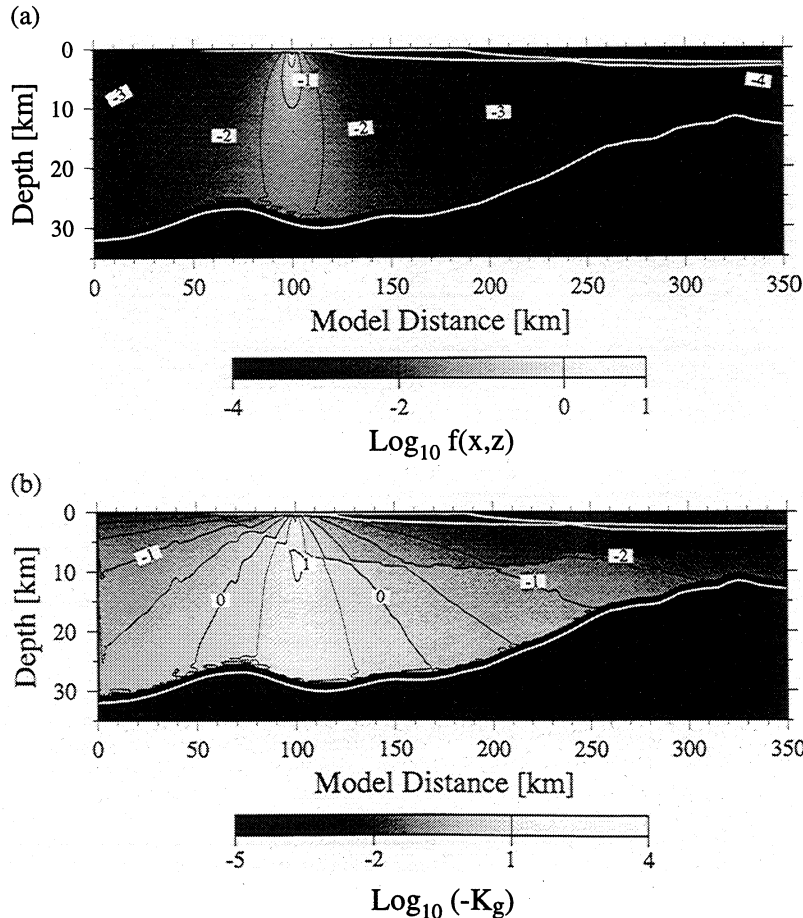

Figure B1. An example of gravity kernel for an input datum located at $x=100$ km and $z=0$ km. (a) Radial part of the gravity kernel, i.e., $f(x,z) = z/(x^2+z^2)$. (b) Total gravity kernel including nodal volume distribution and the slowness derivatives of density. The sensitivity in the sedimentary layer is set to zero for both cases.

slowness and depth components, respectively. The weighting parameters λ_g, λ_v, and λ_d control the significance of the gravity anomaly constraint and the smoothness constraints on the velocity model, respectively, relative to the travel time constraint. The depth-kernel weighting parameter w determines the relative weighting of depth sensitivity in the Fréchet matrices. The details of inversion strategy are identical to those described by *Korenaga et al.* [2000].

To be consistent with the node-oriented parameterization employed by *Korenaga et al.* [2000], the cell volumes of the slowness mesh are redistributed to nodes, and we assign a centroid (x_i, z_i) for each nodal volume of dV_i. The 2-D gravity Fréchet matrix for slowness nodes may be then written as

$$
\begin{aligned}
F_v^{i,j} &= \frac{d\rho}{ds}K(x_i,z_i;x_o^j,z_o^j)dV_i \\
&= 2G\frac{d\rho}{ds}\frac{z_i - z_o^j}{(x_i - x_o^j)^2 + (z_i - z_o^j)^2}dV_i,
\end{aligned} \tag{B2}
$$

where $d\rho/ds$ is the slowness derivative of density, $K(\cdots)$ is a 2-D gravity kernel for a point mass source, and (x_o^j, z_o^j) is an observation point for the jth residual gravity anomaly. Additional sensitivity is required for horizontal edge nodes to be consistent with the padding applied in the forward gravity calculation, so the following sensitivity

$$
\begin{aligned}
F_v^{i,j} = 2G\frac{d\rho}{ds}dz\Bigg[&\frac{(z_i - z_o^j)dx}{(x_i - x_o^j)^2 + (z_i - z_o^j)^2} \\
&+ \frac{\pi}{2} + \tan^{-1}\left(\frac{x_{min} - x_o^j}{z_c - z_o^j}\right)\Bigg],
\end{aligned} \tag{B3}
$$

is applied for the edge nodes at the horizontal minimum of the model domain, x_{min}, based on the semi-infinite slab formula [e.g., *Telford et al.*, 1990]. A nodal volume dV_i is decomposed as $dx\times dz$ in the above expression, and for the nodes at the horizontal maximum, x_{max}, the term $(x_{min} - x_o^j)$ should be replaced with $(x_o^j - x_{max})$. Similarly, the Fréchet matrix for depth nodes, (x_i, z_i), can be derived as

$$
F_d^{i,j} = 2G[\rho(x_i,z_i) - \rho_m]\frac{(z_i - z_o^j)\overline{dx}}{(x_i - x_o^j)^2 + (z_i - z_o^j)^2}, \tag{B4}
$$

where ρ_m is mantle density and $\overline{dx}$ is average distance to neighboring nodes.

An example of the gravity Fréchet matrix for slowness nodes is shown in Figure B1. The radial part of (B2) has strong sensitivity below the observational point with a lateral spread of ~ 15 km, and it rapidly attenuates away from the core (Figure B1a). Because the nodal volume distribution is not regular and gradually increases downward due to the variable grids [see *Korenaga et al.*, 2000, Figure 7] and because different geological subdomains such as the upper and lower igneous crust have different derivatives of slowness with respect to density, the total sensitivity has a few discontinuities and a diffuse character (Figure B1b). Therefore, even after applying a cutoff criterion, the gravity sensitivity matrix is no more sparse. The number of residual gravity anomaly data, however, can be limited because we are interested only in long-wavelength gravity variations, so that it is possible to maintain the memory compactness of the inverse equation.

References

Ahrens, T.J., and G. Schubert, Gabbro-eclogite reaction rate and its geophysical significance, *Rev. Geophys.*, *13*, 383-400, 1975.

Baker, M.B., and E.M. Stolper, Determining the composition of high-pressure mantle melts using diamond aggregates, *Geochim. Cosmochim. Acta*, *58*, 2811-2827, 1994.

Barton, A.J., and R.S. White, Crustal structure of Edoras Bank continental margin and mantle thermal anomalies beneath the North Atlantic, *J. Geophys. Res.*, *102*, 3109-3129, 1997.

Barton, P.J., The relationship between seismic velocity and density in continental crust-A useful constraint?, *Geophys. J. R. Astron. Soc.*, *87*, 195-208, 1986.

Bender, J.F., F.N. Hodges, and A.E. Bence, Petrogenesis of basalts from the project FAMOUS area: Experimental study from 0 to 15 kbars, *Earth Planet. Sci. Lett.*, *41*, 277-302, 1978.

Bernstein, S., High-pressure fractionation in rift-related basaltic magmatism: Faeroe plateau basalts, *Geology*, *22*, 815-818, 1994.

Bernstein, S., P.B. Kelemen, and C.K. Brooks, Highly depleted spinel harzburgite xenoliths in Tertiary dykes from east Greenland: Restites from high degree melting, *Earth Planet. Sci. Lett.*, *154*, 221-235, 1998.

Birch, F., The velocity of compressional waves in rocks to 10 kilobars, part 2, *J. Geophys. Res.*, *66*, 2199-2224, 1961.

Blakely, R.J., *Potential Theory in Gravity and Magnetic Applications*, 441 pp., Cambridge Univ. Press, New York, 1995.

Carlson, R.L., and C.N. Herrick, Densities and porosities in the oceanic crust and their variations with depth and age, *J. Geophys. Res.*, *95*, 9153-9170, 1990.

Carlson, R.L., and G.S. Raskin, Density of the ocean crust, *Nature*, *311*, 555-558, 1984.

Chian, D., C. Keen, I. Reid, and K.E. Louden, Evolution of nonvolcanic rifted margins: New results from the conjugate margins of the Labrador Sea, *Geology*, *23*, 589-592, 1995.

Christensen, N.I., and W.D. Mooney, Seismic velocity structure and composition of the continental crust: A global view, *J. Geophys. Res.*, *100*, 9761-9788, 1995.

Christensen, N.I., and M.H. Salisbury, Structure and constitution of the lower oceanic crust, *Rev. Geophys.*, *13*, 57-86, 1975.

Christensen, N.I., and G.H. Shaw, Elasticity of mafic rocks from the Mid-Atlantic Ridge, *Geophys. J. R. Astron. Soc.*, *20*, 271-284, 1970.

Christensen, N.I., and J.D. Smewing, Geology and seismic structure of the northern section of the Oman ophiolite, *J. Geophys. Res.*, *86*, 2545-2555, 1981.

Christensen, N.I., and R.H. Wilkens, Seismic properties, density, and composition of the Icelandic crust near Raydarfjördur, *J. Geophys. Res.*, *87*, 6389-6395, 1982.

Duncan, R.A., H.C. Larsen, J.F. Allan, and the Shipboard Scientific Party, *Proceeding of the Ocean Drilling Program Initial Report, vol. 163*, Ocean Drilling Program, College Station, Tex., 1996.

Fram, M.S., and C.E. Lesher, Generation and polybaric differentiation of east Greenland early Tertiary flood basalts, *J. Petrol.*, *38*, 231-275, 1997.

Granser, H., Nonlinear inversion of gravity data using the Schmidt-Lichtenstein approach, *Geophysics*, *52*, 88-93, 1987.

Gregory, R.T., and H.P. Taylor Jr., An oxygen isotope profile in a section of Cretaceous oceanic crust, Samail ophiolite, Oman: Evidence for $d^{18}O$ buffering of the oceans by deep (>5 km) seawater-hydrothermal circulation at mid-ocean ridges, *J. Geophys. Res.*, *86*, 2737-2755, 1981.

Grove, T.L., R.J. Kinzler, and W.B. Bryan, Fractionation of mid-ocean ridge basalt (MORB), in *Mantle Flow and Melt Generation at Mid-Ocean Ridges, Geophys. Monogr. Ser.*, vol. 71, edited by J. Phipps Morgan, D. K. Blackman, and J. M. Sinton, pp. 281-310, AGU, Washington, D.C., 1992.

Guspi, F., General 2D gravity inversion with density contrast varying with depth, *Geoexploration, 26,* 253-265, 1990.

Hamilton, E.L., Sound velocity-density relations in sea-floor sediments and rocks, *J. Acoust. Soc. Am., 63,* 366-377, 1978.

Hinz, K., A hypothesis on terrestrial catastrophes wedges of very thick oceanward dipping layers beneath passive continental margins, *Geol. Jahrb., Reihe E, 22,* 3-28, 1981.

Hirose, K., and I. Kushiro, Partial melting of dry peridotites at high pressures: Determination of compositions of melts segregated from peridotite using aggregates of diamond, *Earth Planet. Sci. Lett., 114,* 477-489, 1993.

Holbrook, W.S., and P.B. Kelemen, Large igneous province on the US Atlantic margin and implications for magmatism during continental breakup, *Nature, 364,* 433-436, 1993.

Holbrook, W.S., G.M. Purdy, R.E. Sheridan, L. Glover III, M. Talwani, J. Ewing, and D. Hutchinson, Seismic structure of the U.S. Mid-Atlantic continental margin, *J. Geophys. Res., 99,* 17,871-17,891, 1994a.

Holbrook, W.S., E.C. Reiter, G.M. Purdy, D. Sawyer, P.L. Stoffa, J.A. Austin, Jr., J. Oh, and J. Makris, Deep structure of the U.S. Atlantic continental margin, offshore South Carolina, from coincident ocean bottom and multichannel seismic data, *J. Geophys. Res., 99,* 9155-9178, 1994b.

Hopper, J.R., J.C. Mutter, R.L. Larson, C.Z. Mutter, and Northwest Australia Study Gruop, Magmatism and rift margin evolution: Evidence from northwest Australia, *Geology, 20,* 853-857, 1992.

Horsefield, S.J., R.B. Whitmarsh, R.S. White, and J.-C. Sibuet, Crustal structure of the Goban Spur rifted continental margin, NR Atlantic, *Geophys. J. Int., 119,* 1-19, 1994.

Jordan, T.H., Structure and formation of the continental tectosphere, *J. Petrol., Special Lithosphere Volume,* 11-37, 1988.

Kelemen, P.B., and W.S. Holbrook, Origin of thick, high-velocity igneous crust along the U.S. East Coast Margin, *J. Geophys. Res., 100,* 10,077-10,094, 1995.

Kinzler, R.J., Melting of mantle peridotite at pressures approaching the spinel to garnet transition: Application to mid-ocean ridge basalt petrogenesis, *J. Geophys. Res., 102,* 852-874, 1997.

Kinzler, R.J., and T.L. Grove, Primary magmas of mid-ocean ridge basalts, 2, Applications, *J. Geophys. Res., 97,* 6907-6926, 1992.

Kinzler, R.J., and T.L. Grove, Corrections and further discussion of the primary magmas of mid-ocean ridge basalts, 1 and 2, *J. Geophys. Res., 98,* 22,339-22,347, 1993.

Klein, E.M., and C.H. Langmuir, Global correlations of ocean ridge basalt chemistry with axial depth and crustal thickness, *J. Geophys. Res., 92,* 8089-8115, 1987.

Korenaga, J., W.S. Holbrook, G.M. Kent, P.B. Kelemen, R.S. Detrick, H.C. Larsen, J.R. Hopper, and T. Dahl-Jensen, Crustal structure of the southeast Greenland margin from joint refraction and reflection seismic tomography, *J. Geophys. Res., 105,* 21,591-21,614, 2000.

Korenaga, J., and P.B. Kelemen, Major element heterogeneity of the mantle source in the North Atlantic igneous province, *Earth Planet. Sci. Lett., 184,* 251-268, 2000.

Kuster, G.T., and M.N. Toksöz, Velocity and attenuation of seismic waves in two-phase media, part I, Theoretical formulations, *Geophysics, 39,* 587-606, 1974.

Langmuir, C.H., E.M. Klein, and T. Plank, Petrological systematics of mid-ocean ridge basalts: Constraints on melt generation beneath ocean ridges, in *Mantle Flow and Melt Generation at Mid-Ocean Ridges, Geophys. Monogr. Ser.,* vol. 71, edited by J. Phipps Morgan, D.K. Blackman, and J.M. Sinton, pp. 183-280, AGU, Washington, D. C., 1992.

Larsen, H.C., A.D. Saunders, P.D. Clift, and the Shipboard Scientific Party, *Proceedings of the Drilling Program Initial Report, vol. 152,* Ocean Drill. Program, College Station, Tex., 1994.

LASE Study Group, Deep structure od the US East Coast passive margin from large aperture seismic experiments (LASE), *Mar. Pet. Geol., 3,* 234-242, 1986.

Lizarralde, D., and W.S. Holbrook, U.S. Mid-Atlantic margin structure and early thermal evolution, *J. Geophys. Res., 102,* 22,855-22,875, 1997.

Mavko, G., T. Mukerji, and J. Dvorkin, *The Rock Physics Handbook,* 329 pp., Cambridge Univ. Press, New York, 1998.

McCollom, T.M., and E.L. Shock, Fluid-rock interactions in the lower oceanic crust: Thermodynamic models of hydrothermal alteration, *J. Geophys. Res., 103,* 547-575, 1998.

McKenzie, D., Some remarks on the development of sedimentary basins, *Earth Planet. Sci. Lett., 40,* 25-32, 1978.

Mjelde, R., P. Digranes, H. Shimamura, H. Shiobara, S. Kodaira, H. Brekke, T. Egebjerg, N. Sørenes, and S. Thorbjørnsen, Crustal structure of the northern part of the Vøring Basin, mid-Norway margin, from wide-angle seismic and gravity data, *Tectonophysics, 293,* 175-205, 1998.

Morgan, J.V., and P.J. Barton, A geophysical study of the Hatton Bank volcanic margin: A summary of the results from a combined seismic, gravity and magnetic expriment, *Tectonophysics, 173,* 517-526, 1990.

Morrison, M.A., R.N. Thompson, and A.P. Dickin, Geochemical evidence for complex magmatic plumbing during development of a continental volcanic center, *Geology, 13,* 581-584, 1985.

Mutter, J.C., and C.M. Zehnder, Deep crustal structure and magmatic processes: The inception of seafloor spreading in the Norwegian-Greenland Sea, in *Early Tertiary Volcanism and the Opening of the NE Atlantic,* edited by A.C. Morton and L.M. Parson, pp. 35-48, Blackwell Sci., Malden, Mass., 1988.

Oldenburg, D.W., The inversion and interpretation of gravity anomalies, *Geophysics, 39,* 526-536, 1974.

Parker, R.L., The rapid calculation of potential anomalies, *Geophys. J. R. Astron. Soc., 31,* 447-455, 1972.

Parker, R.L., and S.P. Huestis, The inversion of magnetic anomalies in the presence of topography, *J. Geophys. Res., 79,* 1587-1593, 1974.

Parsons, B., and J.G. Sclater, An analysis of the variation of ocean floor bathymetry and heat flor with age, *J. Geophys. Res., 82,* 803-827, 1977.

Planke, S., Geophysical response of flood basalts from analysis of wire line logs: Ocean Drilling Program Site 642, Vøring volcanic margin, *J. Geophys. Res., 99,* 9279-9296, 1994.

Planke, S., and H. Cambray, Seismic properties of flood basalts from Hole 917A downhole data, Southeast Greenland volcanic margin, *Proc. Ocean Drill. Program Sci. Results, 152,* 453-462, 1998.

Presnall, D.C., S.A. Dixon, T.H. O'Donnell, N.L. Brenner, R.L. Schrock, and D.W. Dycus, Liquidus phase relations on the join Diopside-Forsterite-Anorthite from 1 atm to 20 kbar: Their bearing on the generation and crystallization of basaltic magma, *Contrib. Mineral. Petrol., 66,* 203-220, 1978.

Reid, I., and H.R. Jackson, Crustal structure of northern Baffin Bay: Seismic refraction results and tectonic implications, *J. Geophys. Res., 102,* 523-542, 1997.

Ringwood, A.E., and D.H. Green, Experimental investigations bearing on the nature of the Mohorovicic discontinuity, *Nature, 201,* 566-567, 1964.

Ringwood, A.E., and D.H. Green, An experimental investigation of the gabbro-eclogite transformation and some geophysical implications, *Tectonophysics, 3,* 383-427, 1966.

Roeder, P.L., and R.F. Emslie, Olivine-liquid equilibrium, *Contrib. Mineral. Petrol., 29,* 275-289, 1970.

Schlindwein, V., and W. Jokat, Post-collisional extension of the east Greenland Caledonides: A geophysical perspective, *Geophys. J. Int., 140,* 559-567, 2000.

Smith, W.H.F., and D.T. Sandwell, Marine gravity field from declassified Geosat and ERS-1 altimetry (abstract), *Eos Trans. AGU, 76*(46), Fall Meet. Suppl., F156, 1995.

Sobolev, S.V., and A.Y. Babeyko, Modeling of mineralogical composition, density and elastic wave velocities in anhydrous magmatic rocks, *Surv. Geophys., 15,* 515-544, 1994.

Telford, W.M., L.P. Geldart, and R.E. Sheriff, *Appllied Geophysics,* Cambridge Univ. Press, New York, 1990.

Thompson, R.N., M.A. Morrison, A.P. Dickin, L.L. Gibson, and R.S. Harmon, Two contrasting styles of interaction between basic magma and continental crust in the British Tertiary Volcanic Province, *J. Geophys. Res., 91,* 5985-5997, 1986.

Tréhu, A.M., A. Ballard, L.M. Dorman, J.F. Gettrust, K.D. Klitgord, and A. Schreiner, Structure of the lower crust beneath the Carolina Trough, U.S. Atlantic continental margin, *J. Geophys. Res., 94,* 10,585-10,600, 1989.

Tucholke, B.E., Structure of basement and distribution of sediments in the western North Atlantic Ocean, in *The Geology of North America,* vol. M, *The Western North Atlantic Region,* edited by P.R. Vogt and B.E. Tucholke, pp. 331-340, Geol. Soc. of Am., Boulder, Colo., 1986.

Turcotte, D.L., and G. Schubert, *Geodynamics: Applications of Continuum Physics to Geological Problems,* John Wiley, New York, 1982.

Vogt, P.R., W.-Y. Jung, and J. Brozena, Arctic margin gravity highs remain puzzling, *Eos Trans. AGU, 79,* 601, 605-606, 1998.

Walter, M.J., Melting of garnet peridotite and the origin of komatiite and depleted lithosphere, *J. Petrol., 39,* 29-60, 1998.

White, R., and D. McKenzie, Magmatism at rift zones: The generation of volcanic continental margins and flood basalts, *J. Geophys. Res., 94,* 7685-7729, 1989.

White, R.S., G.D. Spence, S.R. Fowler, D.P. McKenzie, G.K. Westbrook, and A.N. Bowen, Magmatism at rifted continental margins, *Nature, 330,* 439-444, 1987.

Wilkens, R.H., G.J. Fryer, and J. Karsten, Evolution of porosity and seismic structure of upper oceanic crust: Importance of aspect ratios, *J. Geophys. Res., 96,* 17,981-17,995, 1991.

Zehnder, C.M., J.C. Mutter, and P. Buhl, Deep seismic and geochemical constraints on the nature of rift-induced magmatism during breakup of the North Atlantic, *Tectonophysics, 173,* 545-565, 1990.

R. S. Detrick and P. B. Kelemen, Department of Geology and Geophysics, Woods Hole Oceanographic Institution, Woods Hole, MA 02543. (rdetrick@whoi.edu; pkelemen@whoi.edu)

W. S. Holbrook, Department of Geology and Geophysics, University of Wyoming, Laramie, WY 82071-3006. (steveh@uwyo.edu)

J. Korenaga, Department of Earth, Atmospheric, and Planetary Sciences, Massachusetts Institute of Technology, Room 54-512, Cambridge, MA 02139. (korenaga@mit.edu)